



Optimizing an O₂ extraction system to measure atmospheric $\delta^{18}\text{O}$ in ice core

Maureen Eyers Bøge Jørgensen

Master of science thesis

Supervisor: Thomas Blunier

Submitted: 30th June, 2021

Physics of Ice Climate and Earth (PICE), Niels Bohr Institute

ABSTRACT

Understanding past climate changes is important to benchmark and improve future climate model projections. Past climate proxies obtained from sources, such as ice cores, contain a wealth of diverse paleo-environmental information at relatively high temporal resolution.

Isotopic composition of atmospheric O₂ is important for tracing biological and hydrologic processes. Furthermore, measuring $\delta^{18}\text{O}$ conserved in bubbles in ice core can be used a global marker as the time scale for interhemispheric mixing of atmospheric O₂ is one year.

This project focuses on experimental work to reassemble and optimize the O₂ extraction system at Physics of Ice and Climate at the Niels Bohr Institute. The extraction system enables further measurement of atmospheric $\delta^{18}\text{O}$ in ice cores in an Isotope Ratio Mass Spectrometer. Testing of NEEM ice core at the end of the project provided results that were analyzed for further optimizing of the extraction system.

TABLE OF CONTENTS

1	Introduction.....	5
1.1	Ice cores a paleo-environmental archive.....	5
1.2	$\delta^{15}\text{N}$ measurement in ice cores.....	6
1.3	Oxygen cycle and atmospheric oxygen.....	7
1.4	Overview of thesis.....	9
2	Extraction system to measure non-reactive atmospheric gas.....	10
2.1	History of extraction system for discrete N_2 , O_2 , and Ar measurements in ice core.....	10
2.2	Experimental setup.....	11
2.2.1	Pumping system and pressure gauges.....	13
2.2.2	Sample preparation and ice melting.....	14
2.2.3	H_2O and CO_2 trap.....	16
2.2.4	Cryocooler – procedure, passivation and conditioning.....	17
2.2.5	Lines and rods conditioning.....	18
2.2.6	CO_2 trap for standard gas.....	18
3	Isotope ratio mass spectrometry (IRMS) and corrections.....	19
3.1	Mass spectrometry corrections and measurement procedures.....	21
3.1.1	Delta notation and gas standards.....	21
3.1.2	Measurement program.....	22
3.1.3	Zero enrichment test.....	22
3.1.4	Pressure imbalance.....	23
3.1.5	Chemical slope.....	25
3.1.6	Gravitational fractionation.....	26
3.1.7	Thermal fractionation.....	28
3.1.8	Post-coring gas loss fractionation.....	28
4	Results and Discussion.....	29
4.1	abstract.....	29
4.2	Mass spectrometer stability test.....	29
4.3	Dry standard in rod test.....	31
4.4	NEEM results.....	32
4.5	Discussion.....	34
4.5.1	System improvements.....	34
5	Conclusion.....	35
6	REFERENCES.....	36

Acknowledgments

First of all, I would like to express my gratitude to my supervisor Prof. Thomas Blunier for this exciting opportunity to be a part of the gaslab. Furthermore, for the incredible support and patience throughout the duration of this project. I am beyond grateful.

To all my colleagues in the gaslab over all the years. Thank you. In particular, the OGS Gabriella Ciobanu and Sindhu Vudayagiri who were there from the start. Most recently, thank you Rebekka Frøystad, Michael Döring and Michael Dyonisius for working through all the challenges we faced and for making the gaslab an exciting and fun place to be. Especially thank you to Michael Dyonisius for all the support and time you dedicated to navigating the end of this project with me. I am grateful for all the friendships created over the years at CIC and PICE.

Thank you to my family in Canada, UK, and Denmark for always encouraging me to keep moving forward, to never give up. For all the support over the years – I am very grateful.

Kim Bøge Jørgensen, thank you for always supporting me both with this project and for also picking up the slack at home. You have inspired me and challenged me over this project, and I am so grateful for all your love and support.

Most importantly – Hjalte and Asker – this is all for you my loves.

1 INTRODUCTION

1.1 ICE CORES A PALEO-ENVIRONMENTAL ARCHIVE

Understanding past climate changes is important to benchmark and improve future climate model projections (Kageyama et al., 2018). Past climate proxies can be obtained from sources such as ice cores, tree rings, fossil pollen and sediments from oceans. Among these proxies, ice cores are arguably one of the best proxies for Quaternary climate because they contain a wealth of diverse paleo-environmental information at relatively high temporal resolution. For example, polar ice cores have enabled scientists to reconstruct past temperature from water isotopes (e.g., Dansgaard et al., 1969), snow accumulation rates (e.g., Rasmussen et al., 2013), volcanic activity (e.g., Cook et al., 2018) and infer changes in atmospheric circulation (e.g., Buizert et al., 2018).

Ice cores are also unique because the trapped gas air bubbles provide a direct archive of Earth's past atmosphere. Concentration measurements of past greenhouse gases such as carbon dioxide (CO₂) (e.g., Nehrbass-Ahles et al., 2020) and methane (CH₄) (e.g., Rhodes et al., 2015) are critical to constrain Earth's climate sensitivity (Köhler et al., 2017). Isotopic measurements of CO₂ (e.g., Bauska et al., 2016) and CH₄ (e.g., Beck et al., 2018; Dyonisius et al., 2020) from ice cores have been used to infer the sources, sinks, and extent of natural variability of CO₂ and CH₄. Furthermore, concentration and isotopic measurements of these important greenhouse gases provide information on how they responded to and amplified past climate change episodes through various feedback mechanisms.

Other applications of gas measurements in ice cores include measurements of noble gas ratios to reconstruct mean ocean temperature (e.g., Shackleton et al., 2020) and measurements of trace gases such as carbon monoxide (CO) (Faïn et al., 2021), ethane (C₂H₆), and acetylene (C₂H₂) (Nicewonger et al., 2020) to reconstruct past biomass burning activities.

This thesis will focus on gas measurements of ¹⁵N/¹⁴N ratio of molecular nitrogen ($\delta^{15}\text{N}$ of N₂) and ¹⁸O/¹⁶O of molecular oxygen ($\delta^{18}\text{O}$ of O₂) in ice core, both of which are well-established proxies. The novelty of $\delta^{15}\text{N}$ and $\delta^{18}\text{O}_{\text{atm}}$ measurements will be discussed in the following sections. Throughout this thesis, I will use the " $\delta^{18}\text{O}_{\text{atm}}$ " notation to denote the $\delta^{18}\text{O}$ of atmospheric O₂ and prevent the confusion from $\delta^{18}\text{O}$ of water isotopes ($\delta^{18}\text{O}_{\text{ice}}$).

1.2 $\delta^{15}\text{N}$ MEASUREMENT IN ICE CORES

The main compound found in air is nitrogen gas (N_2), which represents 78 % of dry atmosphere. N_2 has an atmospheric residence time of more than 10^7 years so the isotopic composition of N_2 ($\delta^{15}\text{N}$) is constant over the timescale where ice core records are available (Sowers et al., 1989). As snow accumulates, it gradually compacts and densifies into firn and ice (Fig. 1.1.; Herron and Langway, 1980). Although the air bubbles in ice cores contain samples of paleoatmospheric air at the time of pore closure, the composition of gases that are trapped are altered in the firn layer through physical processes such as gravitational and thermal fractionation (Blunier and Schwander, 2000).

The upper part of the firn layer is the convective zone. Here atmospheric pressure changes and variable winds allow for an unimpeded exchange of air between the firn and the atmosphere. In the convective zone $\delta^{15}\text{N}$ does not change. As density in the firn column increases, the free exchange of air in between the firn column and atmosphere starts to decrease. The zone below the convective zone is called is the diffusive zone; here gas diffusion and gravitational fractionation (where gases start to separate based on their masses) starts to occur (Schwander, 1989). In the diffusive zone, $\delta^{15}\text{N}$ in the porosity of the firn begins to change relative to the atmosphere. For a central Greenland site, at a density of 814 kg/m^3 no more change occurs in the value of $\delta^{15}\text{N}$ and bubble close off completes at a density of 830 kg/m^3 (Blunier and Schwander, 2000). Because of its long residence time, alterations in $\delta^{15}\text{N}$ measured in ice cores can be wholly attributed to firn alterations and can be used as a proxy to reconstruct the paleoatmospheric isotopic composition of other gases (Sowers et al., 1989).

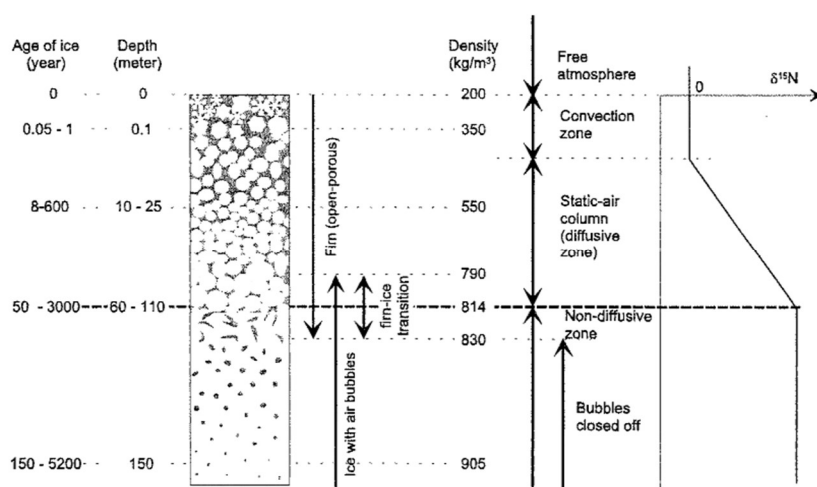


Figure 1.1: The firn layer within the ice column showing the effect of gravitation on $\delta^{15}\text{N}$ with increasing depth. The value of $\delta^{15}\text{N}$ changes linearly with depth increase in the diffusive zone (Blunier and Schwander, 2000)

1.3 OXYGEN CYCLE AND ATMOSPHERIC OXYGEN

Oxygen is the second most abundant gas in the atmosphere and constitutes 20.8 % of the atmosphere. There are three stable oxygen isotopes; the most abundant isotope ^{16}O contributes 99.762% and the two less common, ^{17}O and ^{18}O , contribute 0.038 % and 0.200 % respectively (Emsley, 2011).

Variabilities in the isotopic composition of atmospheric oxygen ($\delta^{18}\text{O}_{\text{atm}}$) is tightly coupled to the water cycle on Earth (Fig. 1.2).

Oxygen in the atmosphere is produced by plants via photosynthesis, which is a process that takes CO_2 and water and turn them into sugar and O_2 . Photosynthesis do not fractionate, i.e., the O_2 produced has the same isotopic composition of O_2 as the source water. On the other hand, atmospheric O_2 is removed via respiration by plants and animals. Respiration preferentially removes ^{16}O relative to ^{18}O – causing $\delta^{18}\text{O}_{\text{atm}}$ to be enriched relative to water. The difference between the oxygen isotope composition of atmospheric oxygen ($\delta^{18}\text{O}_{\text{atm}}$) and ocean water ($\delta^{18}\text{O}_{\text{sw}}$) is known as the Dole effect (Dole, 1935).

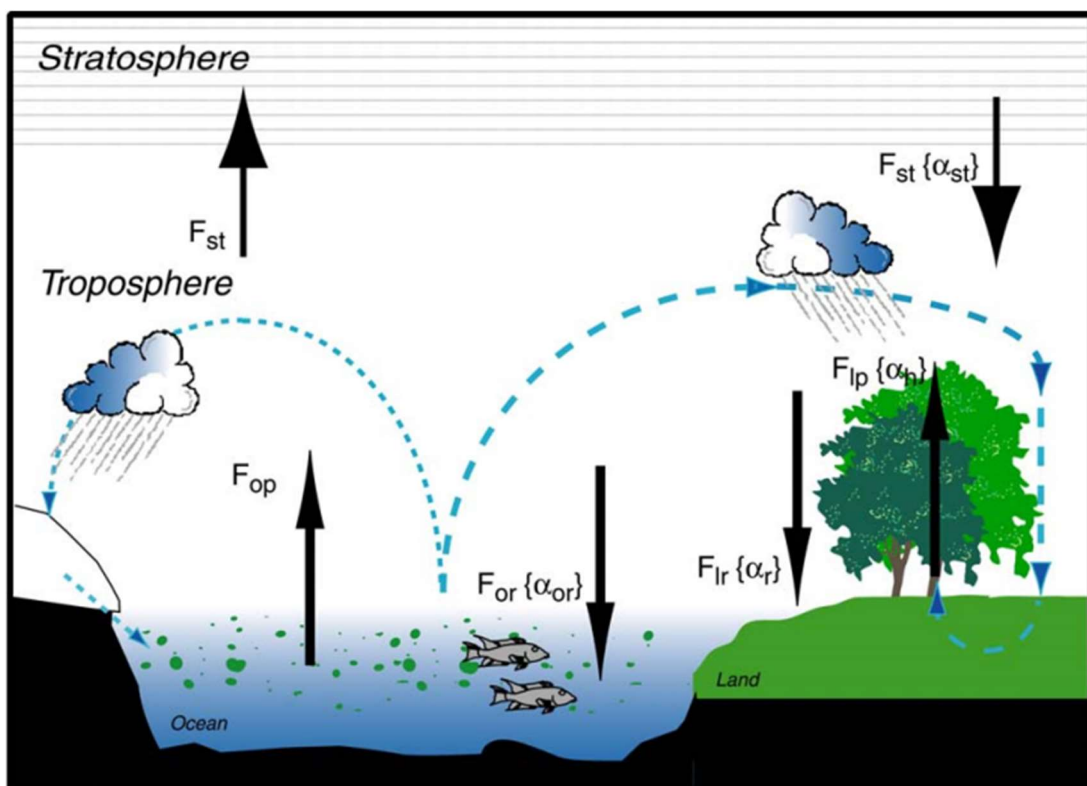


Figure 1.2: The route of oxygen within the marine and terrestrial biospheres and the atmosphere showing the cycle between photosynthesis, transpiration and respiration (Blunier, 2008)

Recent glacial periods on Earth are characterized by decadal to centennial abrupt climate episodes referred to as Dansgaard-Oeschger (D-O) events. A D-O event represents rapid decadal warming in the Northern Hemisphere followed by slow cooling and a bipolar seesaw pattern where the Southern Hemisphere is doing the opposite (rapid cooling followed by slow warming) (WAIS Divide Project Members, 2015). The occurrence of a D-O event is linked to changes in heat transport between the two hemispheres mediated by changes in ocean circulation (Stocker and Johnsen, 2003; Lynch-Stieglitz, 2017).

As the heat balance between the hemispheres changes, a D-O event manifests in the low latitudes as changes in the strength of monsoons and spatial shifts of the tropical rain belt (Wang et al., 2001). It has been argued that the signal from tropical rain belt migration during a D-O event is embedded within the $\delta^{18}\text{O}_{\text{atm}}$ record (Severinghaus et al., 2009; Seltzer et al., 2017). When $\delta^{18}\text{O}_{\text{atm}}$ is normalized to $\delta^{18}\text{O}_{\text{sw}}$ (i.e., when the Dole effect is accounted for), then the remaining changes in $\delta^{18}\text{O}_{\text{atm}}$ reflect changes in where predominant O_2 production from terrestrial photosynthesis is occurring, which in turn driven by latitudinal shifts of the tropical rain belt (Seltzer et al., 2017).

Variations in $\delta^{18}\text{O}_{\text{atm}}$ are also commonly used as a tool to synchronize ice core records (e.g., Capron et al., 2010; Baggenstos et al., 2017). The mixing of air between the Northern and Southern Hemispheres occurs within a 1-year time scale (Sowers et al., 1989), while the long residence time of O_2 (~1200 years) allows for O_2 and its isotopic composition to be well mixed in the atmosphere.

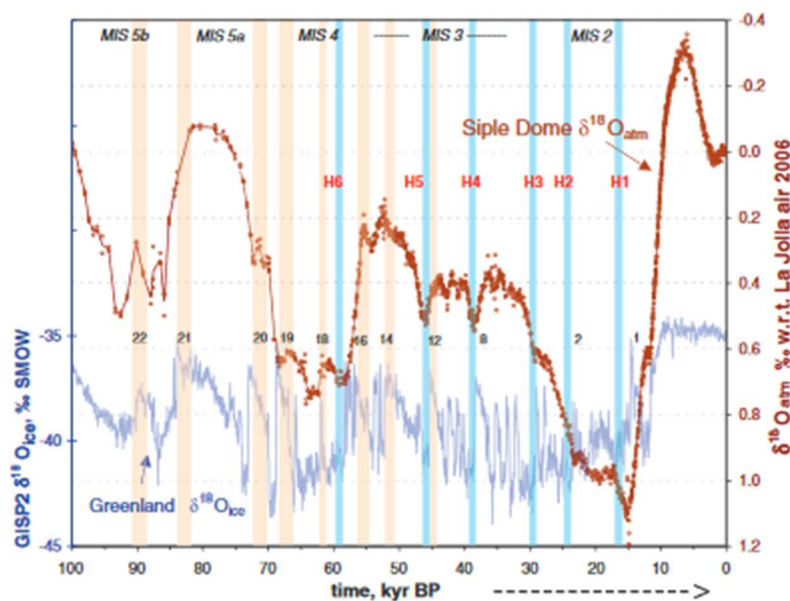


Figure 1.3: Record of the $\delta^{18}\text{O}_{\text{atm}}$ and $\delta^{18}\text{O}_{\text{ice}}$ from the GISP ice core record showing the D-O events marked in black numbers along the plot (Severinghaus et al., 2009).

1.4 OVERVIEW OF THESIS

The original goal of this thesis was to use $\delta^{18}\text{O}_{\text{atm}}$ measurements from Renland ice core (RECAP) (Simonsen et al., 2019) as relative age markers to better establish the RECAP chronology over the Eemian period (70-130 ka). However, the direction of this thesis has been modified over time due to external factors, mostly the laboratory move from Rockefeller building to Tagensvej 16. This thesis now focuses on reassembly and optimization of the O_2 extraction system as well as optimization of the mass spectrometer.

Chapter 2 presents the history of the O_2 extraction system and the aspects of the experimental setup. The focus will be on the various components used in the setup for extraction of gases from ice core and will discuss the process from start to finish. Following, chapter 3 will consider the role of mass spectrometry in measuring $\delta^{18}\text{O}_{\text{atm}}$. The instrument will be introduced, and the procedures discussed for measuring the stable isotopes in the extracted gas. Finally, chapter 4 will present the test ice measured and discuss results and improvements to the overall setup and measurement of $\delta^{18}\text{O}_{\text{atm}}$.

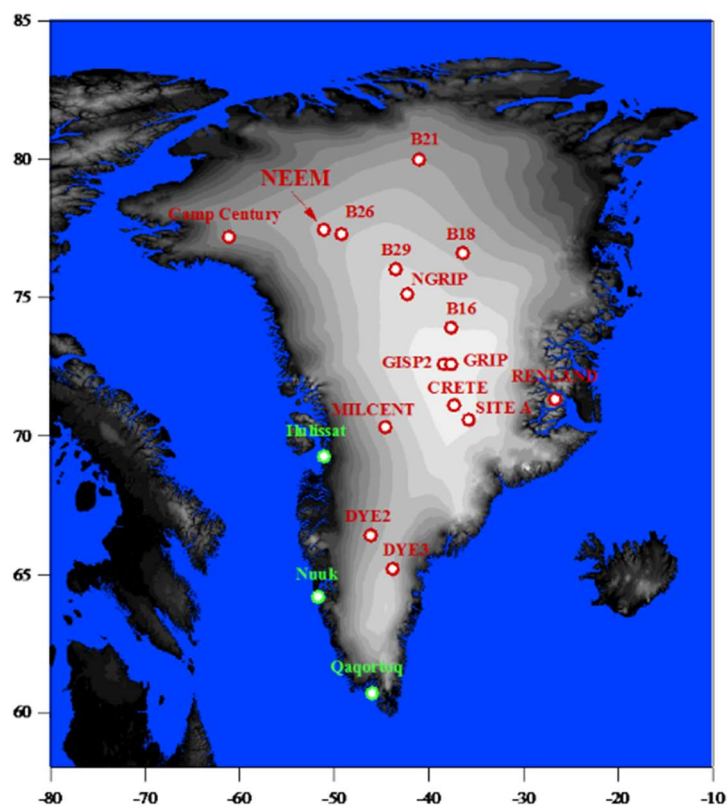


Figure 1.4: A digital elevation model showing locations of Greenland ice core drill projects showing NEEM drilling project in NW Greenland and Renland in East (Masson-Delmotte et al., 2015).

2 EXTRACTION SYSTEM TO MEASURE NON-REACTIVE ATMOSPHERIC GAS

2.1 HISTORY OF EXTRACTION SYSTEM FOR DISCRETE N₂, O₂, AND AR MEASUREMENTS IN ICE CORE

Melt extraction is one of the main techniques used to liberate gas from ice core. Compared to other techniques such as dry extraction with mechanical destruction of the ice (e.g., Jenk et al., 2016) or ice sublimation (e.g., Schmitt et al., 2011), melt extraction is relatively straightforward and has the benefit of almost 100 % extraction efficiency (Sowers et al., 1997). However, one caveat for a melt extraction approach is the effect of gas solubility. Following Henry's law, gas solubility is dependent on the partial pressure of gas over water and temperature. For example, ambient air under an equilibrium condition 14.5 mg/l of oxygen dissolves at 0 °C water as compared to 7.6 mg/l dissolving at 20 °C water (Emsley, 2011). A common method to drive off all the gases that is dissolved in the meltwater back to the extraction chamber headspace is to slowly refreeze the meltwater (e.g., Sowers et al., 1989). This method is commonly known as a melt-refreeze method.

Due to its simplicity, melting is generally preferable for analysis of gases with low solubility that also do not chemically react with the meltwater in ice core. Traditionally, this means everything except CO₂ mole fraction and isotope measurements. The first measurement of paleoatmospheric $\delta^{18}\text{O}_{\text{atm}}$ from Camp Century ice core in Greenland was presented by Horibe et al. (1985). Sowers et al. (1989) described a system that was able to measure $\delta^{15}\text{N}$ of N₂ and O₂, N₂, Ar molecular ratios in addition of $\delta^{18}\text{O}_{\text{atm}}$ with a very simple melt-refreeze extraction setup and a collection unit made of stainless-steel tube dipped in liquid helium (Fig. 2.1). Further investigations showed that the presence of H₂O and CO₂ in the sample interferes with isotopic measurements (Headly, 2008); thus, additional cryogenic H₂O and CO₂ traps are commonly introduced between the extraction setup and the collection unit (Petrenko et al., 2006; Oyabu et al., 2020). Methods to accurately measure Ar isotopes and elemental ratios Ar/N₂, O₂/N₂, Ar/O₂, are described by Severinghaus et al. (2003). The setup for accurately measure Ar isotopes necessitates additional removal of O₂ and N₂ via gettering (destroying all the reactive gas in the sample by reaction with "getter" Zr/Al) (Severinghaus et al., 2003).

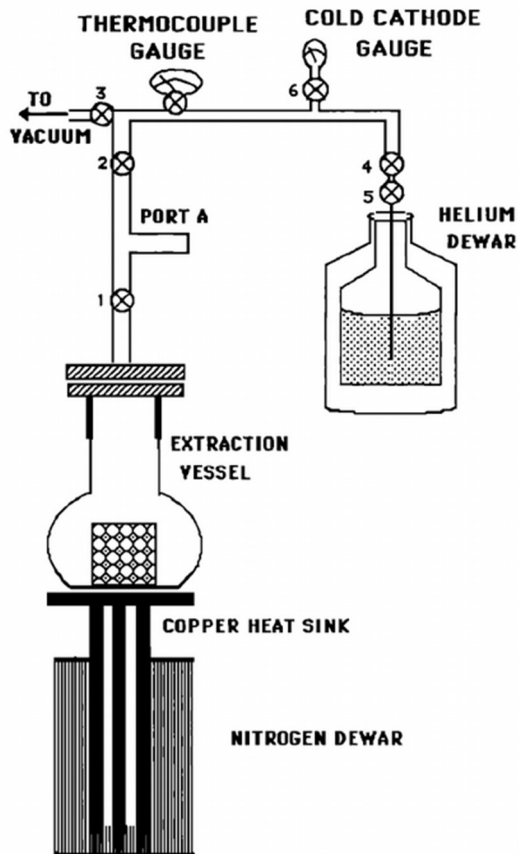


Figure 2.1: Original wet extraction system used to extract enclosed gases from ice. The extracted gases is then collected inside dip tubes at liquid helium temperature (adapted from Sowers et al., 1989)

2.2 EXPERIMENTAL SETUP

This thesis builds upon the work initially done by Reutenauer (2016). The extraction system starts with the ice melting/gas extraction section (Section 2.2.2) and ends with a collection unit (Section 2.2.4; Fig. 2.2). Between the ice melting section and the collection unit, water and CO₂ traps are used for purification of the gas sample (Section 2.2.3). In addition to the sample line, there is also a secondary pumping line necessary to evacuate remaining gas and water vapor in the line between samples (Section 2.2.1). The system is controlled using a LabView program/graphical user interface. The LabView program allows for opening and closing of pneumatic valves and monitoring of vacuum pressure through the two pressure gauges (Fig. 2.3a and Fig. 2.3b).

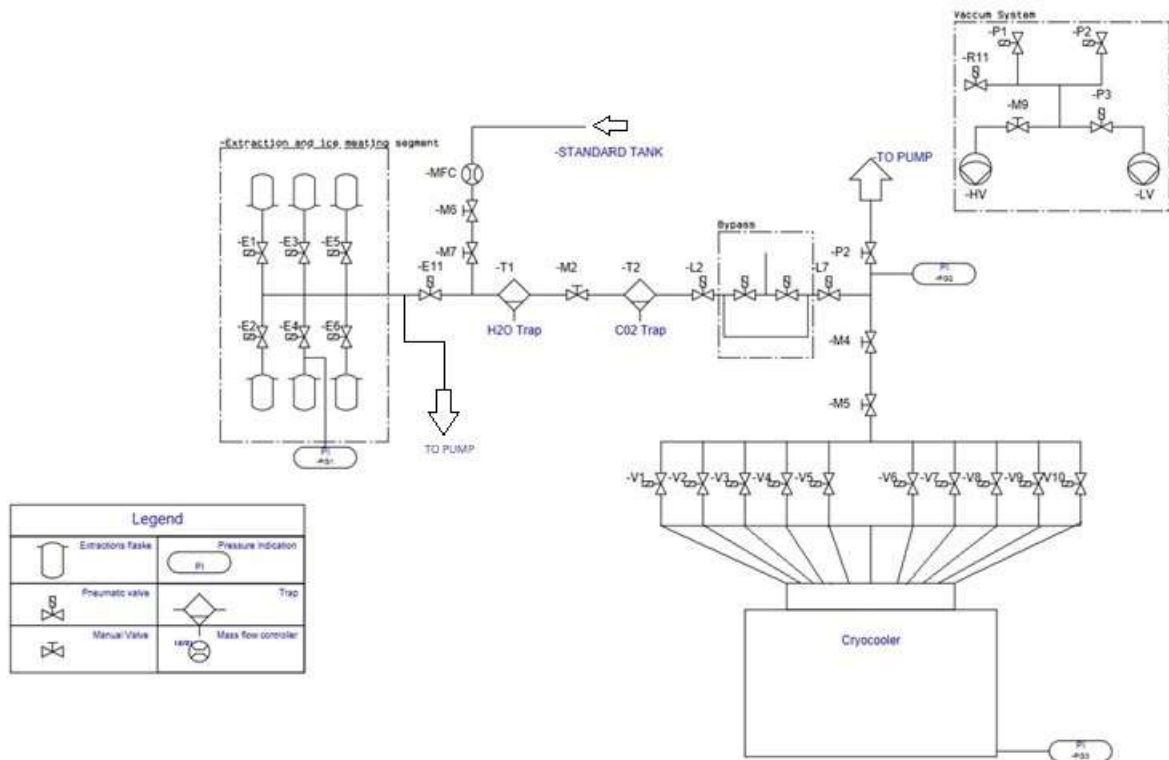


Figure 2.2: PCSchematic drawing of extraction system with pump lines in inset (Joergensen, 2021).

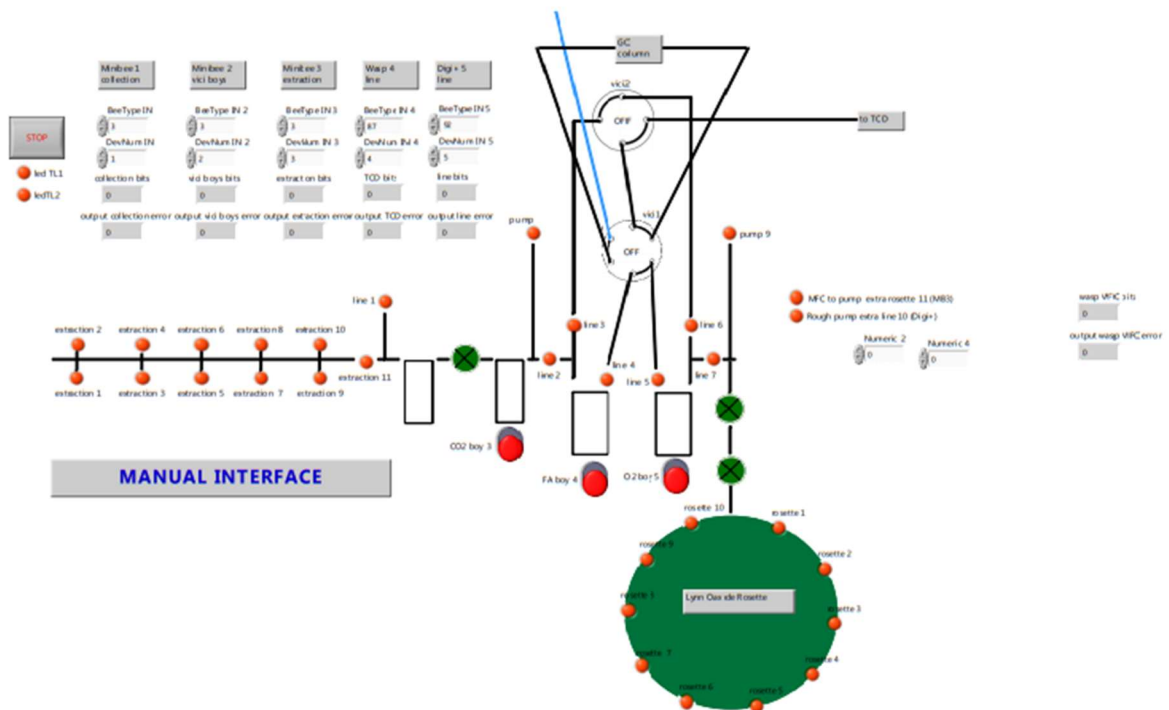


Figure 2.3a – Semi-automated LabView user interface controlling pneumatic valves in the extraction lines and the collection unit (Reutenauer, 2016).

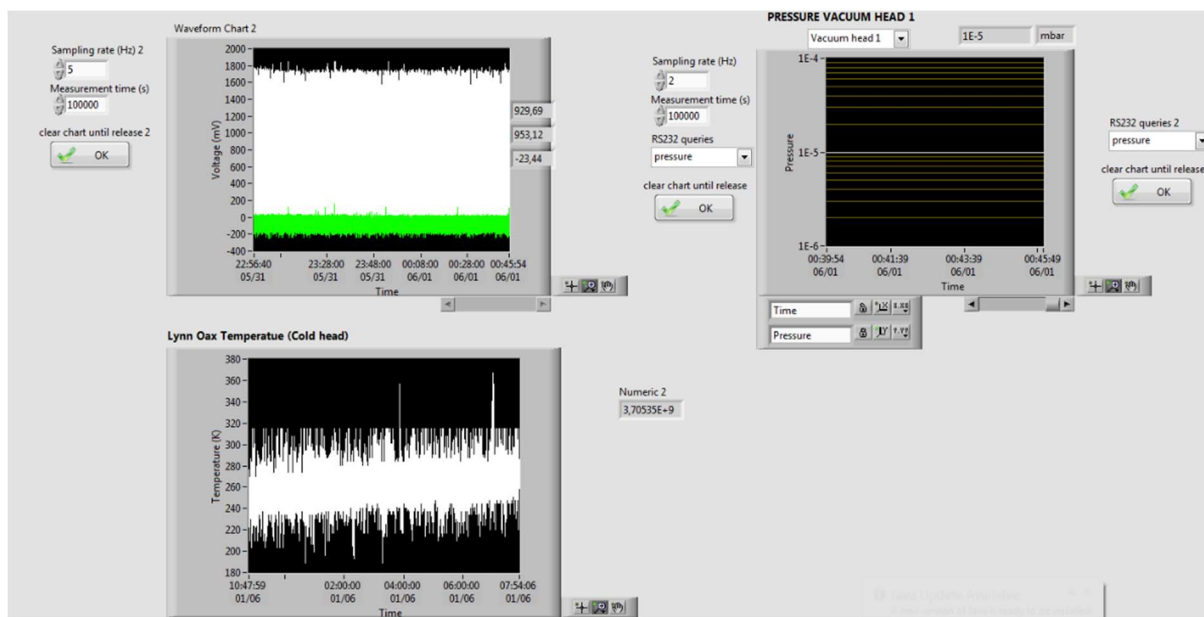


Figure 2.3b – LabView user interface displaying pressure readout for PG1 and PG2 (not shown) and temperature of coldhead (cryocooler) (designed and developed by(Reutenauer, 2016)).

2.2.1 Pumping system and pressure gauges

The pumping system is not part of the sample line but provides crucial function to allow the evacuation of ambient air from the line and extraction vessel. The pumping system consists of two pumps, a “rough” rotary vane pump and a high-vacuum turbomolecular pump station (Hi-Cube, Pfeiffer Vacuum, Germany). The turbomolecular pump unit also includes an oil-free diaphragm pump which is connected to the main extraction lines (1/4” stainless steel tubes) and collection unit (Fig. 2.2). The pressure in the system is read on Pirani gauges “PG1” and “PG2” through the LabView program. An additional pressure gauge “PG3” is connected to the lower side of the vacuum casing in the collection unit. The vacuum casing in the collection unit is evacuated using the rotary vane rough pump as the need for low vacuum is not necessary. The pressure monitored on “PG3” is displayed on a digital readout from the Hi-Cube pumping station.

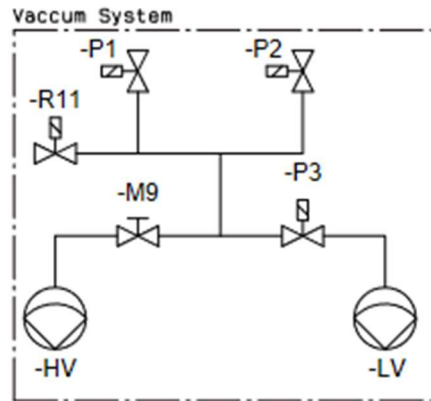


Figure 2.4: PCSchematic diagram of pumping system showing connection between pumps, extraction lines and collection unit HV represents Hi-Cube turbomolecular pump and LV represents “rough” rotary vane pump (Joergensen, 2021).

2.2.2 Sample preparation and ice melting

The ice samples are moved from the main storage facility at Priorparken (-28 °C) to the working freezer at NBI-PICE (-20 °C) weeks before the planned extraction date. The ice samples are cut to a length of approximately 6 cm and a mass of approximately 40 g from the bulk ice core using an electric band saw inside the -20 °C freezer (Fig. 2.5). Approximately 0.5 cm of ice is cut from the surface of the sample; first with the electric band saw and then additional 1-2 mm by using a ceramic knife. This procedure not only ensures that any contaminants such as drill fluid are removed from the surface, but also enables more accurate measurements for paleoatmospheric reconstruction due to removal of ice surfaces that would have experienced diffusive gas loss during storage (Oyabu et al., 2020). All handling of the samples is done using powder-free nitrile gloves to prevent contamination.

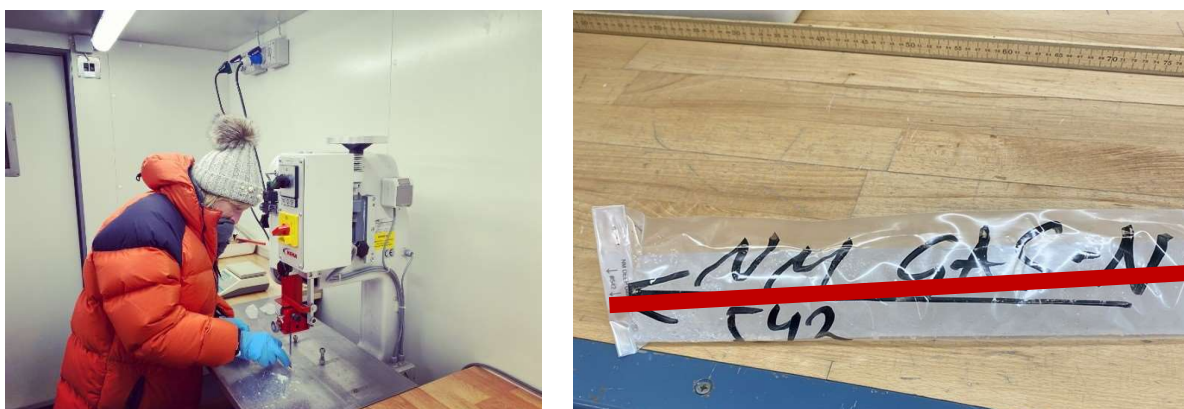


Figure 2.5: In house freezer with electric bandsaw used to trim ice (left) and NEM ice sample (right) with red line representing ~40 cm.

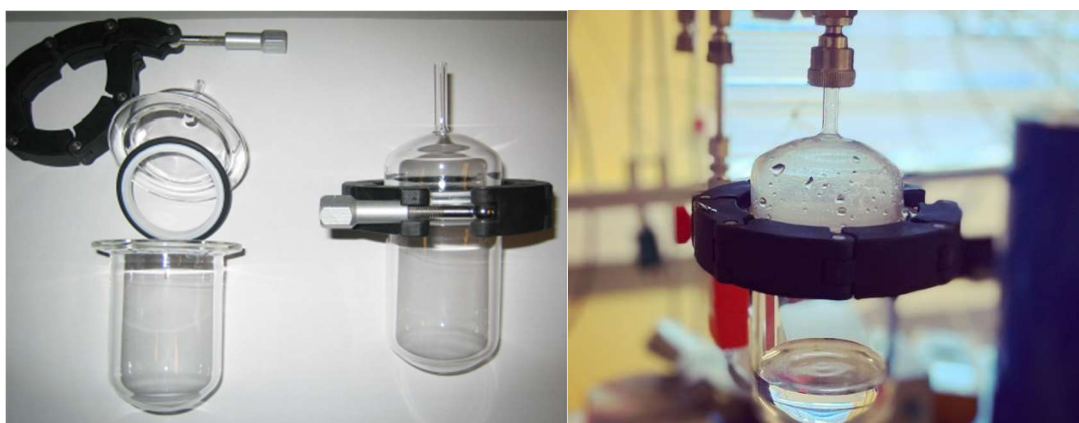


Figure 2.6: Extraction flasks with rubber O-ring and Swagelock Ultra-Torr 1/4-inch connector designed to optimize exchange between melt water from ice sample and head space. The upper section of the flask attaches to the extraction line and the lower, cylindrical (reproduced from Reutenauer, (2016))

Glass extraction flask with 210 cm³ volume (Reutenauer, 2016) is used as a container where the ice is melted. Sample flask treatment begins two days before the planned extraction. The flasks are first cleaned using ethanol and Milli-Q™ water. Then they are left overnight in a 50 °C oven to dry. Several hours before melting, the flasks are moved to the same freezer as the samples, which is cooled to -20 °C. The Viton O-rings and connector are cleaned in the same manner as the glass flasks, but they are not placed in the oven or the freezer to prevent damage to the material.

Prior to extraction and melting the lines are evacuated for 20 minutes using the rotary vane pump and followed by 10 minutes with the turbomolecular pump. This enables a vacuum pressure of 10⁻⁵ mbar to be reached. The extraction vessel is attached to the extraction line using a Swagelock Ultra-Torr 1/4-inch connector that contains a Viton O-ring to seal the connection (Fig. 2.6). The flask is submerged in a pre-chilled ethanol bath at -24 °C. Submerging the flask in cold ethanol prevents premature melting of the ice sample as ambient air is evacuated away from the headspace. The ambient air in the flask is then evacuated initially using the rotary vane pump then followed by pumping with the turbomolecular pump for 10 minutes. This pumping step has the additional benefit of making the sample cleaner, as it sublimates away a few milligrams of potentially dirty ice on the surface of the sample. During evacuation, pressure in the flask is usually at vapor pressure of ice (between 5-10 mbar, depending on temperature of ice, Fig. 2.7).

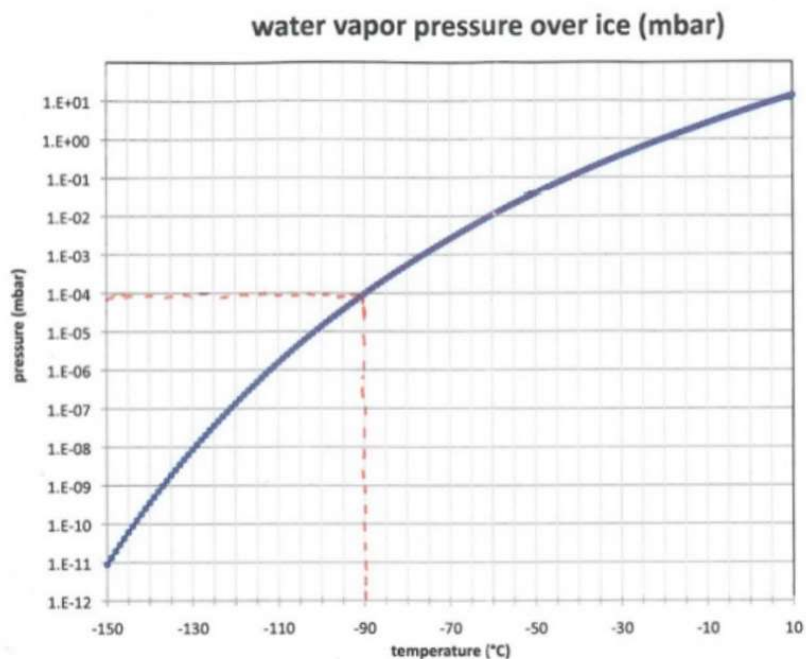


Figure 2.7: Vapor pressure over ice as a function of temperature (modified from Murphy et al., (2005)).

After the evacuation step is complete, the ice is melted with a warm water bath that is maintained at a temperature of +45°C. The flask is gradually submerged to prevent melting too quickly and clogging the water trap. To minimize the solubility effect, the gas released from melting of the ice is actively pumped and transferred into the collection unit following Oyabu et al.(2020). The melt vessel is taken out of the warm water bath when ~5g of ice is left. Removing the warm water bath early prevents overheating of the meltwater from the ice and reduces the possibility of contamination from reaction between the meltwater and impurities in the ice. After all the ice is visibly melted, the gas is transferred into the collection unit for an additional 15 minutes to ensure complete gas transfer.

2.2.3 H₂O and CO₂ trap

The gas released from the melted ice is pulled through the lines and first pass through a H₂O trap. This trap is a stainless-steel cylinder, ~20 cm in length with a diameter of ~5 cm. The H₂O trap is filled to ¾ full with 2mm glass beads. These beads provide an increased surface area for water vapor. Removing water vapor is necessary because it tends to “stick” on metal surfaces for long and can alter the isotope signature of O₂ via isotope exchange (Reutenauer, 2016).

The H₂O trap is cooled using a mixture of ethanol and liquid nitrogen to a temperature of -80°C. The ethanol is pre-cooled with the Thermo NESLAB cold finger prior to the addition of liquid nitrogen.

Although the exact mechanism is still unknown, it is known that the presence of CO₂ interferes with $\delta^{18}\text{O}_{\text{atm}}$ and $\delta^{15}\text{N}$ measurements (Headly, 2008). One hypothesis that could explain the CO₂ interference is that CO₂ acts as intermediary catalyst for formation of NO_x in the ion source. Among the NO_x families, ¹⁴N¹⁸O, ¹⁵N¹⁷O, and ¹⁵N¹⁸O directly interferes with the oxygen cups (m33 and m34) (Headly, 2008). Thus, the CO₂ in the sample is trapped cryogenically using a simple 1/8" stainless steel U-trap at liquid nitrogen (-196 °C) temperature. The trap is submerged in a dewar filled with liquid nitrogen. The dewar is controlled through LabView and is raised up and down to a control point as needed. The trap acts as a secondary H₂O trap to remove any residual water vapour that was not removed in the first trap as freezing point of H₂O (atmospheric pressure) is 0 °C. During the transition between ice samples, the CO₂ trap is heated with a hairdryer while the sample line is evacuated to prevent clogging of the CO₂ trap.

2.2.4 Cryocooler – procedure, passivation and conditioning

The sample collection unit is described in detail by Reutenauer (2016). In brief, the unit consists of a closed-cycle helium cryocooler and 10 stainless steel rods (Fig. 2.8). Surrounding the rod manifold is a vacuum casing with the lower section of the rods placed on a copper block. The vacuum casing is evacuated through the rough pump and is always evacuated prior to operating the equipment. The pressure in the casing, which is measured with "PG3" (Fig. 2.2), is evacuated to less than 10⁻³ mbar. The cold head is cooled using a Sumitomo water cooled helium (He) compressor which removes the heat away from the copper block and allows the temperature of the collection rods to be as low as 10K. A temperature of this level is necessary as oxygen and nitrogen have freezing temperatures of 54 K and 63 K, respectively. The pressure and temperature gradient between the cooled rods and the ice extraction vessel drive the gas transfer. Once all of the gas has been solidified into the rods, all valves on the manifold are closed and the rods are heated to approximately 250 – 270 K for 30-45 minutes to allow the gas in the rods to equilibrate before measurement.

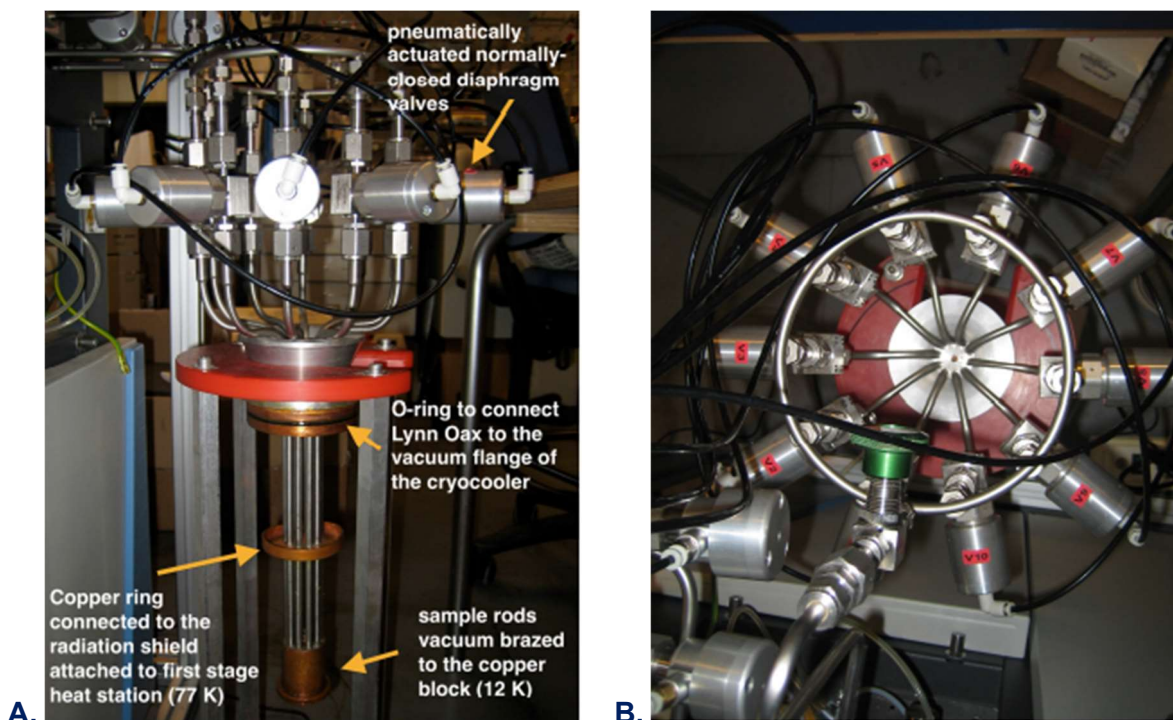


Figure 2.8: A. Internal view of cryocooler with pneumatic valves on top and stainless steel rods, B. Overview of the 10 pneumatic valves connected to the rods (modified from (Reutenauer, 2016)).

2.2.5 Lines and rods conditioning

If a sample extraction is not scheduled for a particular day, then the rods are conditioned with NEEM 2 standard (clean background modern air) and left overnight. This ensures that the surface of the rods is conditioned with a gas that has an isotopic composition closely resembling the samples. Conditioning the rods is necessary because the stainless-steel surface of the rods continuously desorb and adsorb gases. These processes can alter the isotopic composition of the samples (see Chapter 4).

2.2.6 CO₂ trap for standard gas

As discussed previously, the presence of CO₂ in sample mixture interferes with $\delta^{18}\text{O}$ and $\delta^{15}\text{N}$ (Headly, 2008). In Reutenauer (2016) only CO₂ from the sample is removed. In this project the CO₂ from the standard gas is also removed via ascarite trap added between the standard NEEM tank and the outer MS valves.

3 ISOTOPE RATIO MASS SPECTROMETRY (IRMS) AND CORRECTIONS

This chapter will present the background on the instrument used for the measurements and will discuss the corrections done to the data. The project uses a Thermo Delta V Plus Isotope Ratio Mass Spectrometer (IRMS). The IRMS consists of four primary sections: the ion source, acceleration, deflection, and finally the detector section (Fig. 3.1). The ion source consists of a heated tungsten filament that ionizes the sample molecules. The ion beam produced in the source is accelerated by focusing electric plates and deflected by a magnetic field. The deflection is dependent on the mass to charge (m/z) ratio of the molecules.

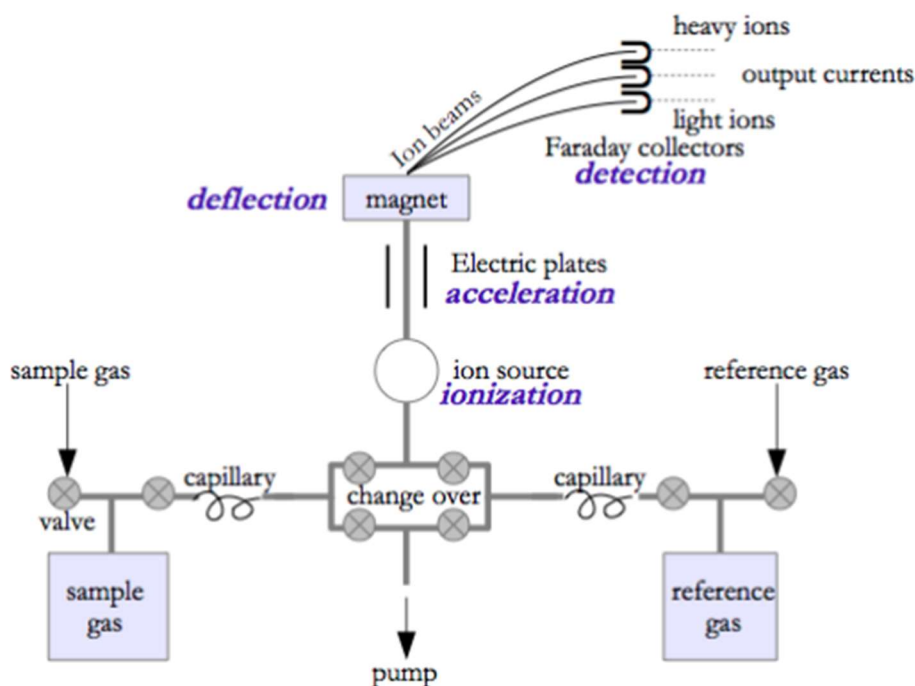


Figure 3.1: Schematic diagram of dual inlet system in the IRMS, showing two separate bellows and the pathway of gas through the changeover, ionization and acceleration sections to the final detection in the faraday cups (Guillevic et al., 2014).

The kinetic energy of the charged particles through the magnetic field is a product of the charge (q) and the voltage difference (V) (Equation 3.1). In this equation, v is the velocity of the charged isotope and mass (m) representative of the mass to charge ratio.

$$\frac{1}{2}mv^2 = Vq \quad (3.1)$$

Deflection into these cups is dependent on the trajectory of the charged particles relative to radius of curvature, with heavier isotopes having a longer radius of curvature than lighter isotopes (Equation 3.2).

$$r = \sqrt{\frac{2mV}{qB^2}} \quad (3.2)$$

The detector section of the Delta V Plus IRMS used in this study is equipped with 7 Faraday cups (Table 3.1). The cup configuration enables mass measurements (m/z) 28, 29, 32, 33, 34, 36 and 40 for the “N₂/O₂/Ar” configuration and (m/z) 28, 29, and 30 for the “N₂” configuration.

The dual inlet system (Fig. 3.1) enables measurement of sample and standard gases in two separate adjustable volume/bellows. With the adjustable bellows, signal intensity in the detector can be made equal for both standard and sample (Leuenberger 2008). During measurement, the sample and standard gases are flown from the bellows through crimp capillaries, which act as flow reducer, into the changeover manifold. The changeover manifold has valves that alternate between being opening to the source or to the waste pump, allowing for sample and standard gases from the two bellows to be introduced to the source sequentially.

Table 3.1: Cup configuration for Delta V Plus MS used in this study

Cup #	1	2	3	4	5	6	7
Slit width (mm)	1.4	1.4	3.8	1.4	3.8	1.4	1.4
(m/z) N2/O2/Ar configuration	28		32	33	34	36	38
(m/z) N2 configuration			28	29	30		
Resistor (ohm) N2/O2/Ar	3 E ⁸		1 E ⁹	1 E ¹²	3 E ¹¹	1 E ¹²	1 E ¹⁰
Resistor (ohm) N2			3 E ⁸	3 E ¹⁰	1 E ¹¹		

3.1 MASS SPECTROMETRY CORRECTIONS AND MEASUREMENT PROCEDURES

3.1.1 Delta notation and gas standards

When comparing values between stable isotopes, the ratio can be quite small, resulting in values being compared to the thousands. Most MS therefore calculate abundance of isotopes in delta notation (δ , ‰, per mil) (Slater et al., 2001). This notation was introduced to be able to make comparisons more readily to parts per thousand (per mil) (Craig, 1961). The following equation represents the isotopic ratio calculation for $\delta^{18}\text{O}$:

$$\delta^{18}\text{O} = \left(\frac{(^{18}\text{O}^{16}\text{O}/^{16}\text{O}_2)_{\text{sample}}}{(^{18}\text{O}^{16}\text{O}/^{16}\text{O}_2)_{\text{standard}}} - 1 \right) \cdot 10^3 \text{‰} \quad (3.3)$$

Following Severinghaus et al. (2009) a modern background air is used for $\delta^{15}\text{N}$ and $\delta^{18}\text{O}_{\text{atm}}$ standard. For this project, dried atmospheric air collected from NEEM camp in northwest Greenland, stored in a stainless-steel tank was used. The standard NEEM air can be introduced either directly from the tank to the right-hand side “standard” bellow of the dual inlet system for the zero enrichment test (Section 3.1.4) or through the extraction lines similar to the sample.

3.1.2 Measurement program

The automation scripts for sample measurements were originally developed at University of California, San Diego (UCSD). The automation scripts was modified by Corentin Reutenauer (NBI) (Reutenauer, 2016) and throughout this project. The following parameters were used for each measurement cycle (an example of sequence shown in Appendix A):

- (1) Two blocks of zero enrichment measurements (section 3.2.3), one with N₂/O₂/Ar configuration and one with N₂.
- (2) Each rod containing a sample is measured in three blocks, two with N₂/O₂/Ar configuration and one with N₂.
- (3) Zero enrichment measurements are repeated after two sample measurements.
- (4) Each block contains 16 cycles with integration time of 16 seconds.

3.1.3 Zero enrichment test

In a zero enrichment test, both bellows are filled with the same standard gas and measured against each other. This test represents an idealized measurement condition and is used to gauge the instrument internal precision and drifts. Fig. 3.2 shows the zero enrichment tests conducted up to 2 weeks before the measurement of the NEEM test ice. All values for $\delta^{18}\text{O}$ and $\delta^{15}\text{N}$ are below zero which could possibly be a result of fractionation within the bellows, in particular the sample bellow, resulting in an enrichment of lighter isotopes within the bellow.

The pooled standard deviation was calculated to for both $\delta^{18}\text{O}$ and $\delta^{15}\text{N}$ results. For $\delta^{18}\text{O}$ the result is 0,037 ‰ and $\delta^{15}\text{N}$ is 0,060 ‰. These values represent the internal precision of the MS.

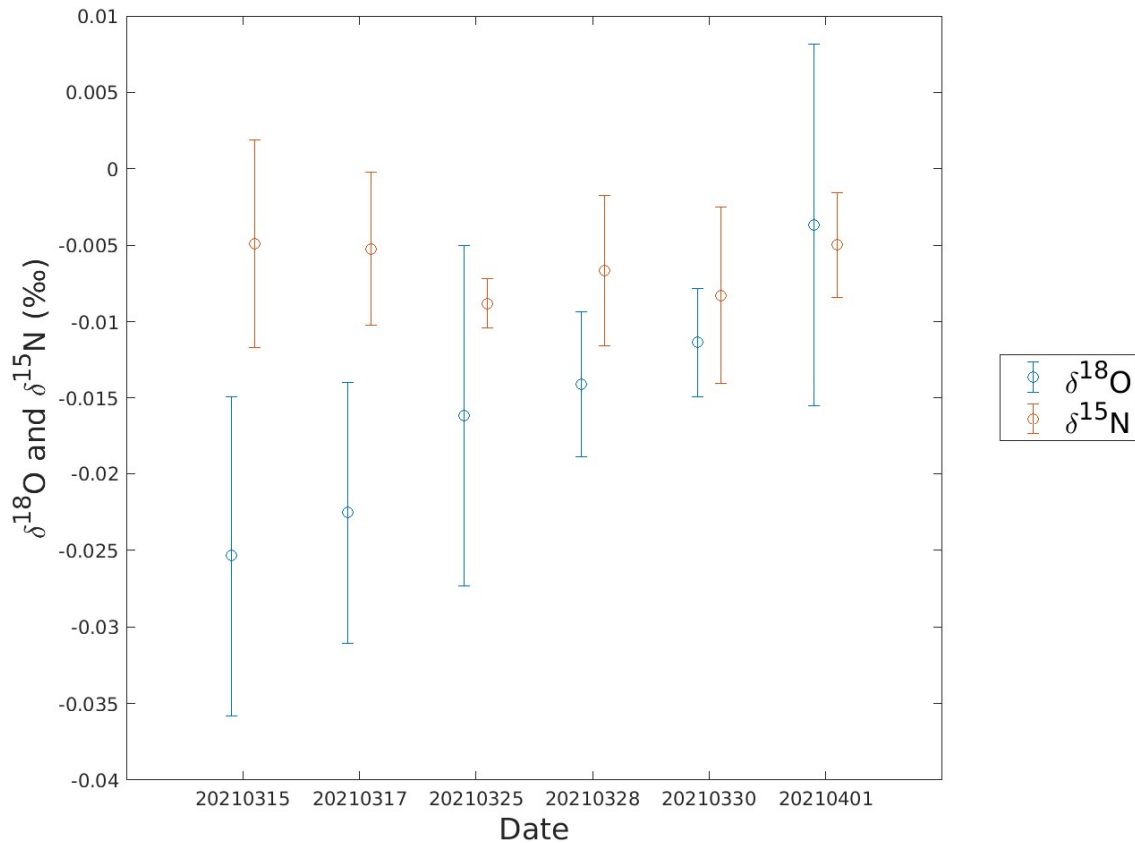


Figure 3.2: Zero enrichment results from 15 March, 2021 to 1 April, 2021. The results show that the $\delta^{18}\text{O}$ and $\delta^{15}\text{N}$ values are below zero for all measurements over these weeks.

3.1.4 Pressure imbalance

The slight difference in pressure of the bellows can affect the measured $\delta^{18}\text{O}_{\text{atm}}$ and $\delta^{15}\text{N}$ values. The amount standard gas introduced into the reference bellow is set manually by a pressure regulator attached to the tank. Generally, the amount of standard gas in the reference bellow is adjusted to be relatively close to the sample. However due to varying total air content in ice core samples, there will always be slight offsets between the measured intensity of the sample and standard (ΔI).

To measure the effect of pressure imbalance, an experiment similar to the zero enrichment test is conducted but with the pressure in the sample bellow being intentionally offset compared to the standard bellow. Both bellows are filled with the same amount of standard gas and the volume of the sample bellow is adjusted at 5% interval for every measurement. The measured $\delta^{18}\text{O}$ from this test is usually plotted against the difference in intensity (ΔI) (Fig. 3.4); from the slope of ($\delta^{18}\text{O}$ vs. ΔI), a linear correction for the samples can be developed using the following equation:

$$\delta^{18}\text{O}_{\text{pressure corrected}} = \delta^{18}\text{O}_{\text{measured}} - (\text{PI slope}) * \Delta I \quad (3.4)$$

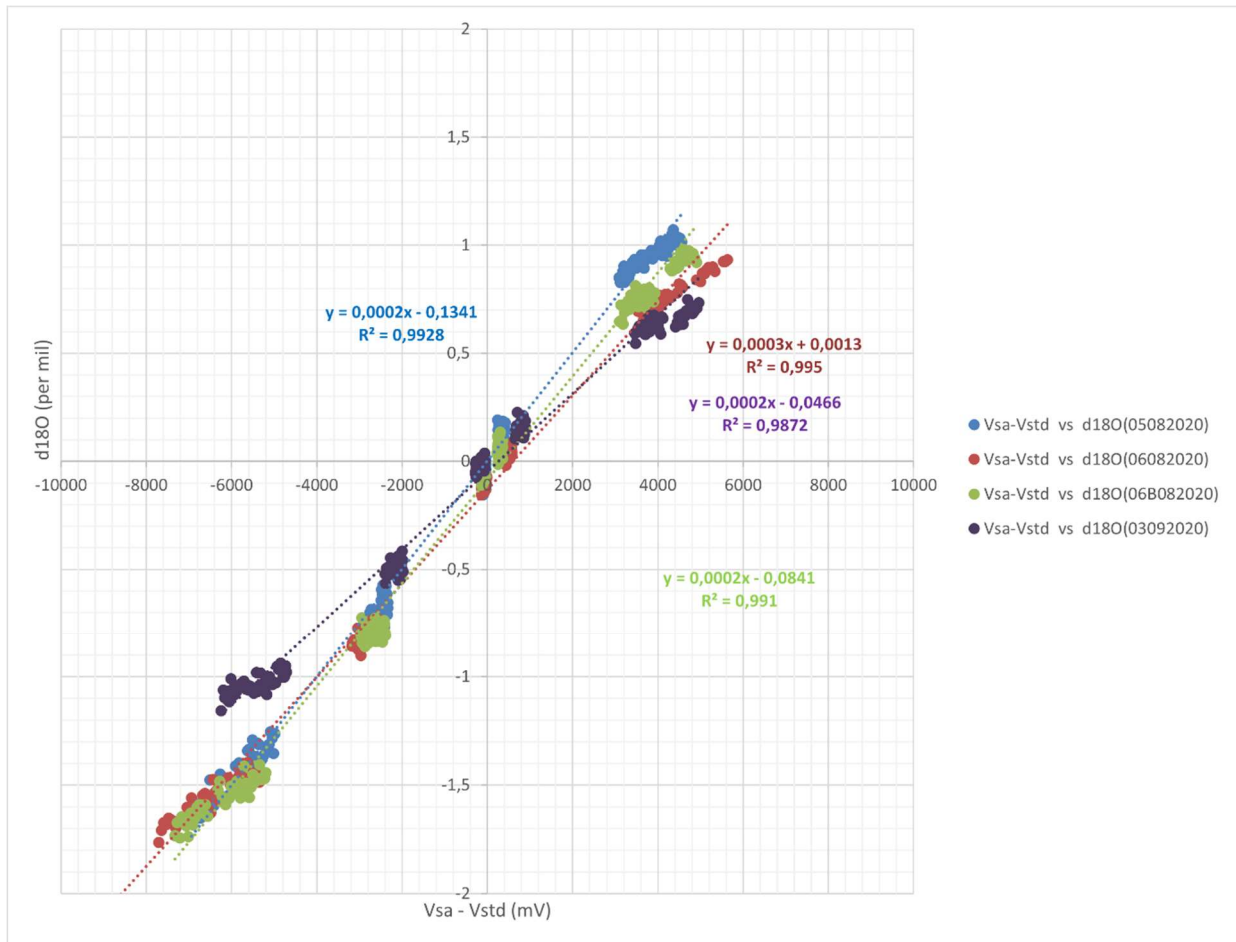


Figure 3.4: Pressure imbalance results for testing weeks end of 2020. R^2 values range between 0.9872 and 0.995. The slope (used in equation 3.1) ranges between 0.0003 and 0.0002. Dates of measurements are in brackets to the right of the plot (day.month.year).

Pressure imbalance measurements are done typically at the beginning of a measurement week. Fig. 3.4. shows the variability in the slope of pressure imbalance tests over one month. Fig. 3.5. Shows the last pressure imbalance test conducted before NEEM test ice measurements presented in this thesis.

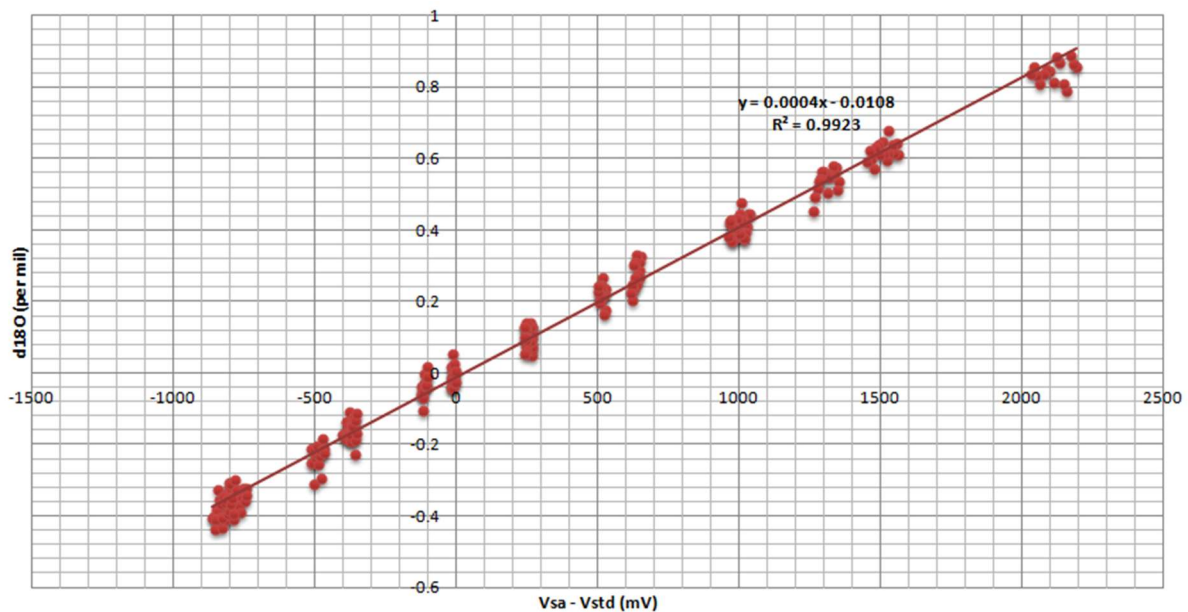


Figure 3.5: Pressure imbalance results for measurement week (8 April, 2021). R^2 value, shown on plot, is 0.9923. The slope (used in equation 3.1) is 0.0004.

Pressure imbalance test was also conducted for $\delta^{15}\text{N}$ by Frøystad (2021). The ($\delta^{15}\text{N}$ vs. ΔI) relationship was found to be small, so the $\delta^{15}\text{N}$ measurements were not corrected for pressure imbalance.

3.1.5 Chemical slope

In air mixtures, variations in elemental ratios can impact the isotopic ratio. For example, variations in $\delta\text{O}_2/\text{N}_2$ of the sample influences the measured $\delta^{18}\text{O}$ (Severinghaus et al., 2003). This is mostly because the relative abundance of other gases affect the ionization efficiencies of the gas isotopes differently (Severinghaus et al., 2003). To compensate for this phenomenon, a chemical slope test is conducted. A method from Kindler, (2013) is adapted in this study. A chemical slope test starts with the introduction of ultrapure N_2 at low pressure (2-3 mbar) into the sample bellow and NEEM standard into the reference bellow ($\sim 38\text{-}40$ mbar). Rather than alternating gases from the two bellows, here during “sample” measurement the two valves leading to bellows are open simultaneously into the source. This procedure allows for dynamic mixing in the changeover manifold before the gas reaches the source. The sample bellow (N_2) is subsequently compressed throughout the measurement to enrich the gas in the source with N_2 .

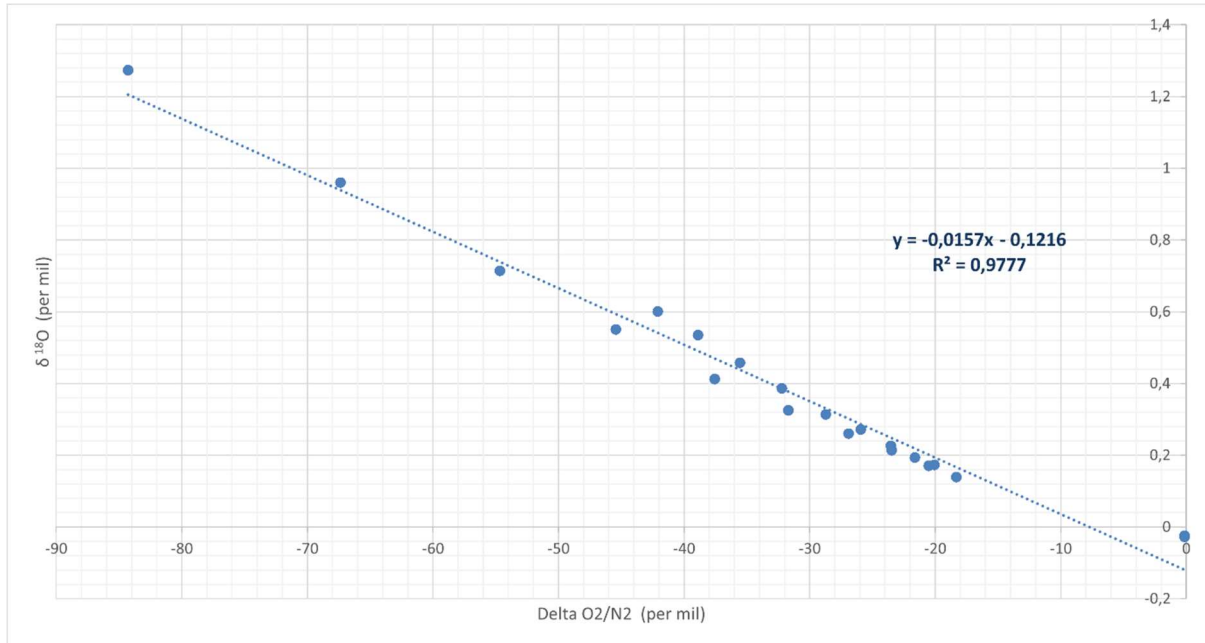


Figure 3.6: Chemical slope for pure N₂ for the measurement week. The resultant slope will be used in equation 3.1.

The linear regression resulting from δ¹⁸O versus δO₂/N₂ in a chemical slope test can be used to calculate the necessary correction (Fig. 3.6). The slope from this linear regression provides the sensitivity of δ¹⁸O to δO₂/ N₂ ratio following:

$$\delta^{18}\text{O}_{\text{chemical slope}} = \delta^{18}\text{O}_{\text{pressure corrected}} + (\text{chemical slope}) * \delta\text{O}_2/\text{N}_2 \quad (3.5)$$

Chemical slope test δ¹⁵N against δO₂/N₂ was also conducted in Frøystad (2021). Similar to the pressure imbalance, the (δ¹⁵N vs. δO₂/N₂) relationship was found to be small, so the δ¹⁵N measurements were not corrected for chemical slope.

3.1.6 Gravitational fractionation

Due to gravity, heavy isotopes in the open porosity of the firn preferentially gather at the bottom of the firn column. This results in the bubbles within the firn and ice to be enriched with heavier isotopes (Schwander, 1989). The gravitational fractionation is derived following barometric equation (Craig et al., 1988):

$$\frac{R}{R_0} = e^{g \cdot z \cdot \frac{\Delta m}{R^*}} \quad (3.6)$$

where

R = measured isotope or gas ratio

R₀ = measured isotope or gas ratio for free atmosphere

g = acceleration due to gravity

z = thickness of firn layer

Δm = difference in mass between the two isotopes

R* = gas constant

T = isothermal temperature within the column

This formula then shows that the difference in mass between two isotopes will affect the gravitational fractionation. Because of the 2 amu (atomic mass unit) differences, δ¹⁸O will be twice as affected by gravitational fractionation as δ¹⁵N (Craig et al., 1988). Alterations in δ¹⁵N measured in ice cores can be attributed exclusively to firn effects and mass-dependent fractionation during sample extraction. Thus, measurements of δ¹⁸O can be corrected for all mass-dependent processes (including gravitational fractionation) following

$$\delta^{18}\text{O}_{\text{corrected}} = \delta^{18}\text{O}_{\text{meas}} - 2 * \delta^{15}\text{N}_{\text{meas}} \quad (3.7)$$

where δ¹⁸O_{meas} and δ¹⁵N_{meas} are the measured δ¹⁸O and δ¹⁵N corrected for all instrument effects (zero enrichment, pressure imbalance, and chemical slope

3.1.7 Thermal fractionation

Heavier elements tend to favour colder areas; therefore, the temperature gradient within the firn influences where these elements are distributed (Grachev, 2013). Large scale temperature changes (for example during DO events) can cause large temperature gradients within the firn column and result in thermal fractionation (Landais et al., 2004). However, the NEEM test ice measured in this project is from the Holocene (0-2000 yrs before present). During this time period temperature variations were relatively low. Thus, for the purpose of this study, thermal fractionation does not need to be considered.

3.1.8 Post-coring gas loss fractionation

Gas loss in ice core can occur during sample storage. Fractionation due to gas loss can be associated with size-dependent fractionation and mass-dependent fractionation (Bender et al., 1995). Size-dependent fractionation can occur when overpressure on the bubbles during storage causes diffusion of gases through the ice lattice, excluding smaller molecules. This can significantly affect the measured elemental ratios such as O_2/N_2 and Ar/N_2 (Bender et al., 1995).

Gas loss correction is specific to a particular ice core, and even specific drilling season because it depends on sample handling and storage history (Severinghaus et al., 2009; Baggenstos et al., 2017). An ideal way to correct for gas loss is to measure recent Holocene ice from the same ice core of interest. After all the corrections described above, the $\delta^{18}O_{atm}$, $\delta O_2/N_2$ and $\delta Ar/N_2$ in recent Holocene ice relative to modern air should be 0‰. Any deviations in the measured $\delta^{18}O_{atm}$, $\delta O_2/N_2$ and $\delta Ar/N_2$ can be attributed to post-coring gas loss. Thus, an empirical correction using linear relationship between corrected $\delta^{18}O_{atm}$, $\delta O_2/N_2$ and $\delta Ar/N_2$ can be made to correct for gas loss.

The samples in this study are not corrected for gas loss due to several reasons. First, the NEEM ice core was drilled recently (NEEM Community Members, 2013) thus the post-coring gas loss should be minimal. Second, as discussed in the following chapter there are more pressing analytical issues in the system that prevent accurate reconstruction of $\delta^{18}O_{atm}$, $\delta O_2/N_2$ and $\delta Ar/N_2$.

4 Results and Discussion

4.1 ABSTRACT

The results presented in this thesis cover the test experiments done during the reassembly of the oxygen measurement system, in preparation to measure the RECAP core. The MS stability test uncovers the problem that potentially explain why the internal precision of the MS was not as good as before the laboratory move. The dry standard in rod test shows that after significant downtime, the unconditioned stainless steel rods can introduce significant amount of uncertainty to the $\delta^{18}\text{O}$ measurement. Finally, the NEEM test ice measurements suggest that alteration of sample gas in the stainless steel rods might be worse in presence of water vapor. Suggestions to further optimize the system are discussed.

4.2 MASS SPECTROMETER STABILITY TEST

As discussed in Section 3.1.3, from the zero enrichment test the internal precision of the MS was worse than the precision achieved by Reutenauer (2016). To test the stability of the MS, the standard bellow was filled with large amount of standard air (~200 mbar). The standard air then flown into the source overnight and continuous MS measurements were made under the N₂/O₂/Ar configuration. Fig. 4.1 show the result of overnight stability test.

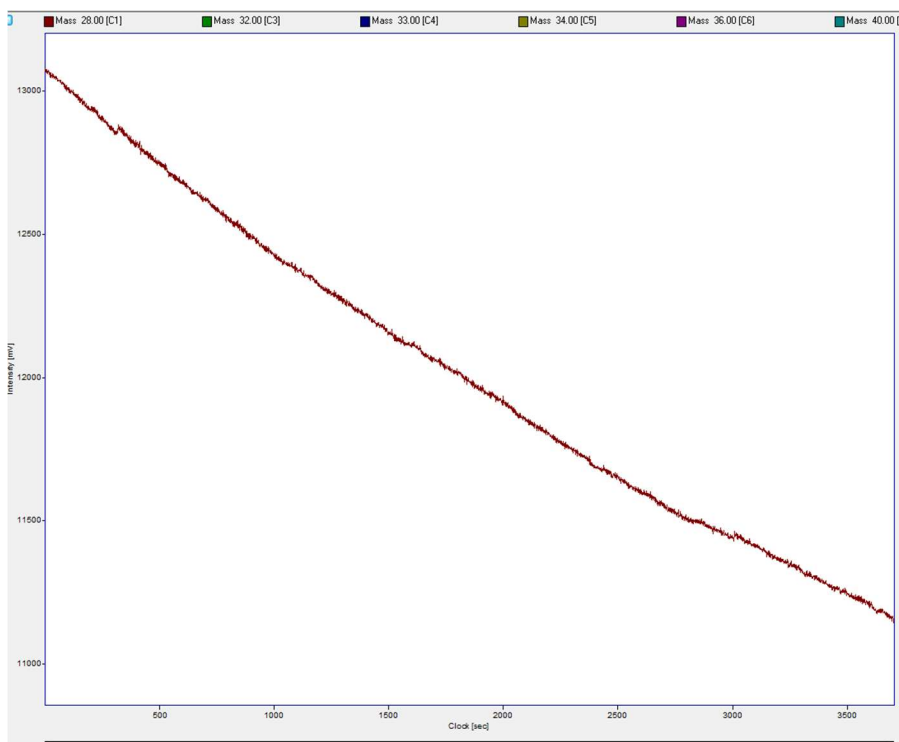


Fig 4.1: Intensity versus time for mass 28 showing the high frequency noise.

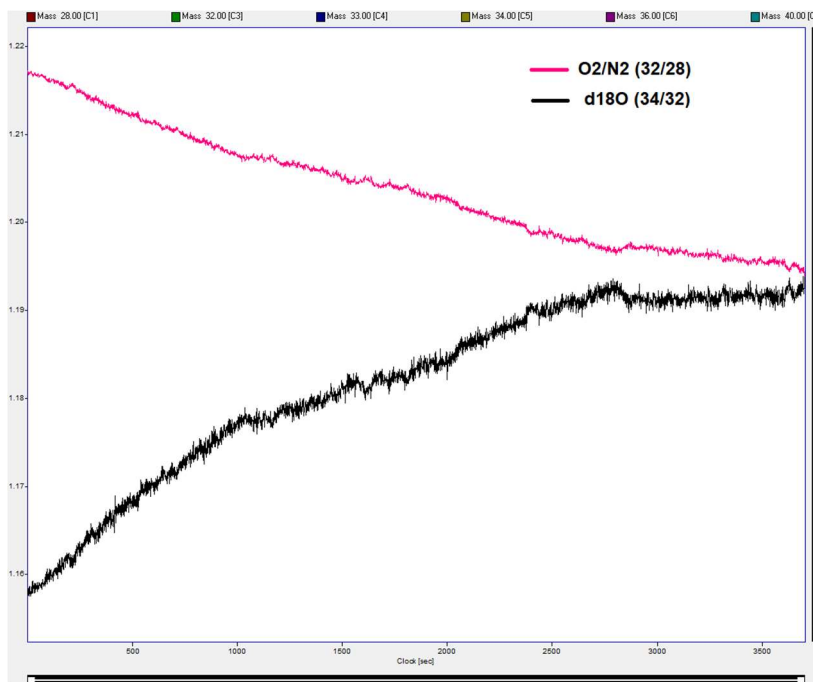


Figure 4.2: Noise in intensity versus time scan for $\delta^{18}\text{O}$ and O_2/N_2 .

The intensity decrease over time is expected from sample consumption. However, the overnight sensitivity test show that there was significant high frequency noise on all masses. $\delta\text{O}_2/\text{N}_2$ and $\delta^{18}\text{O}$ measurements (Fig. 4.2) from the overnight test show similar high frequency noise superimposed on significant drifts in measured ratios.

One solution tried was to swap out the source in the MS. However, the source change did not remove the high frequency noise. An intensity vs. high voltage scan show that the high frequency noise was related to narrow peak shapes; thus, small instabilities in ion beam can cause significant variabilities in measured intensity. The narrow peak shapes suggest either the Faraday cups in the detector were out of position (R. Beaudette, Scripps Institute of Oceanography Laboratory Technician, personal communication) or magnetic field interference likely due to damage to the magnetic section (M. Leuenberger, University of Bern Professor, personal communication).

One suggestion from Thermo technical support to improve instrument stability is to install stainless steel shims in the flight tube. The shims improve the peak shapes for one week before the narrow peak shapes return. A temporary solution to this problem was to adjust the "extraction %" parameter within the focus settings. This improved the peak shapes and internal precision, although at the time of writing, even with low extraction % parameter the internal precision still 50% worse than achieved by Reutenauer (2016) (0.037 permil vs. 0.005 permil).

4.3 DRY STANDARD IN ROD TEST

To account for any effects of sample alteration in the rods, standard gas was introduced into the rods through the sample line at 4 standard cc per minute using the mass flow controller (MFC). Similar to the sample, the standard was also run through the CO₂ trap. The ten rods were measured against the same NEEM standard in the MS. Under ideal conditions, the measured $\delta^{18}\text{O}$ values from the rods should be zero as the gas being measured is the same in the standard bellow. Observing the difference in the results allows for us to see the influence of the rods on sample measurements.

These measurements were performed by Frøystad (2021) over a period of two months (Fig 4.3). The results showed which rods were not performing well. Table 4.1 presents an example of standard in rod measurements for the week of melting NEEM. The rods that have the most unreliable measurements are rods 10, 5, 4 (highlighted in red). These rods were not used during NEEM test ice extraction.

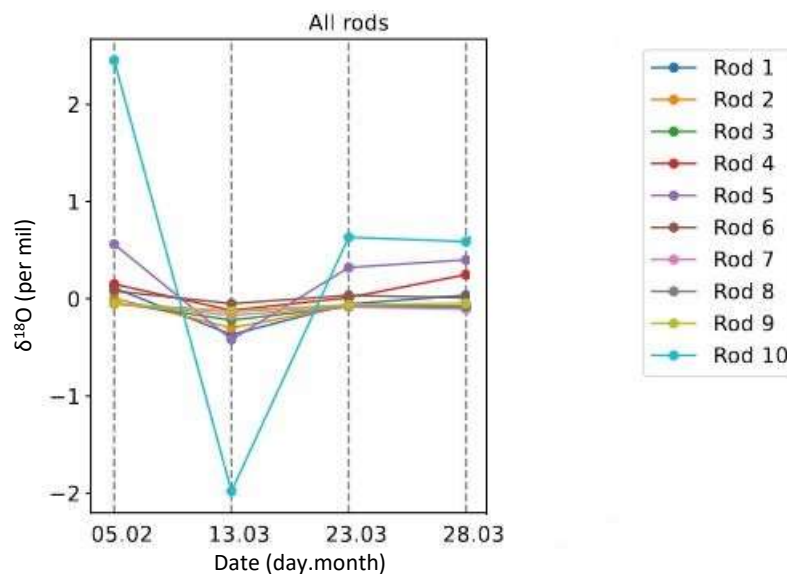


Figure 4.3. All rod measurements from February 2021 to beginning of measurement week. Froystad (2021) shows rods with the greatest compromise (in particular rod 10). Based on these results decisions were made to use rods 8,6,1,9 and 3 for NEEM measurements (modified from Froystad (2021)).

Table 4.1 Standard in rods for measurement week of NEEM ice

Date	d18O/16O (per mil)	d15N/14N (per mil)	Rod #
28 March	-0,107	-0,049	7
	0,587	0,380	10
	-0,082	-0,035	2
	0,036	0,032	1
	-0,078	-0,041	3
	0,010	0,022	6
	-0,046	-0,029	9
	0,400	0,252	5
	0,247	0,164	4
	-0,086	-0,035	8

4.4 NEEM RESULTS

NEEM is recently drilled ice core so the expected results should reflect present day atmospheric gas composition. Shallow NEEM should be approximately from 1000 AD. The expected values for $\delta^{15}\text{N}$ should be 0.27 per mil due to the minimum firn depth changes. Results for $\delta^{18}\text{O}$ should have a value of zero after corrections for gravitational fractionation are calculated. The elemental ratio for O_2/N_2 should also have results of zero.

Table 4.2 shows the measured and corrected values for two consecutive NEEM test ice measurement days. The measured $\delta^{18}\text{O}$ is corrected for pressure imbalance ($\delta^{18}\text{O}_{\text{PI}}$, Equation 3.4, slope = 0,0004, chemical slope ($\delta^{18}\text{O}_{\text{cs}}$, Equation 3.5, slope = 0,0157), zero enrichment ($\delta^{18}\text{O}_{\text{ze}}$) and gravitational fractionation ($\delta^{18}\text{O}_{\text{grav}}$). Due to operator error, no gas made it to rod #8 on 1/4/21 test. Thus rod #8 is omitted when considering standard deviation calculations. Standard deviation (σ) calculations were done for the samples measured between all the rods as well as each rod over the two days (Table 4.3).

Table 4.2 Results from 2 consecutive NEEM measurement days

A. 1 April 2021

Rod #	$\delta^{18}\text{O}_{\text{raw}}$ (per mil)	$\delta^{18}\text{O}_{\text{PI}}$ (per mil)	$\delta^{18}\text{O}_{\text{CS}}$ (per mil)	$\delta^{18}\text{O}_{\text{ze}}$ (per mil)	$\delta^{18}\text{O}_{\text{grav}}$ (per mil)	$\delta^{15}\text{N}_{\text{raw}}$ (per mil)	$\delta^{15}\text{N}_{\text{ze}}$ (per mil)	$32\text{O}_2/28\text{N}_2$ (per mil)
8	-55,068	2,758	1,934	1,922	26,517	-12,306	-12,298	52,462
6	0,498	0,988	1,111	1,098	0,742	0,170	0,178	-7,817
1	0,929	0,994	1,239	1,223	0,497	0,358	0,363	-3,606
9	0,588	0,989	1,046	1,030	0,520	0,250	0,255	-3,606
3	0,021	0,933	0,863	0,854	0,343	0,043	0,255	4,429

B. 30 March 2021

Rod #	$\delta^{18}\text{O}_{\text{raw}}$ (per mil)	$\delta^{18}\text{O}_{\text{PI}}$ (per mil)	$\delta^{18}\text{O}_{\text{CS}}$ (per mil)	$\delta^{18}\text{O}_{\text{ze}}$ (per mil)	$\delta^{18}\text{O}_{\text{grav}}$ (per mil)	$\delta^{15}\text{N}_{\text{raw}}$ (per mil)	$\delta^{15}\text{N}_{\text{ze}}$ (per mil)	$32\text{O}_2/28\text{N}_2$ (per mil)
8	0,308	0,991	0,966	0,980	0,715	0,120	0,133	1,628
6	0,354	1,004	1,134	1,147	1,014	0,054	0,067	-8,248
1	0,868	1,024	1,256	1,268	0,547	0,349	0,361	-14,771
9	0,567	0,997	1,056	1,068	0,517	0,264	0,275	-3,736
3	0,242	0,988	1,021	1,030	0,720	0,151	0,155	-2,125

The standard deviation for measurements 1 April 2021 for $\delta^{18}\text{O}_{\text{gravitation}}$ was 0,164 (per mil) and 0,076 (per mil) for $\delta^{15}\text{N}_{\text{zero enrichment}}$.

The standard deviation for measurements 30 March 2021 for $\delta^{18}\text{O}_{\text{gravitation}}$ was 0,228 (per mil) and 0,118 (per mil) for $\delta^{15}\text{N}_{\text{zero enrichment}}$.

Table 4.3 Standard deviation (σ) for each rod between the two days

Rod #	8	6	1	9	3
$\sigma \delta^{18}\text{O}_{\text{gravitation}}$	18,245	0,193	0,036	0,002	0,267
$\sigma \delta^{15}\text{N}_{\text{zeroenrichment}}$	8,790	0,079	0,002	0,014	0,071

Over the two measurement days, rods 9 and 1 show the 'best' results (closest to zero). Rod 9 results for 1 April 2021, for $\delta^{18}\text{O}_{\text{grav corrected}} = 0,5196$ (per mil) and with $\sigma = 0,001782$ for the two measurements in that rod. The results for for 30 March 2021, for $\delta^{18}\text{O}_{\text{grav corrected}} = 0,5170$. However, these results are clearly not reliable as the test ice measurements on the same rods are remarkably similar. This suggests that significant alteration of sample gas occurred in the rods, causing a large "memory effect." Because this memory effect is not present in dry rod

measurements, I hypothesize that the presence of water vapor (from the ice extraction) might exacerbate the alteration of sample gas in the rods.

4.5 DISCUSSION

4.5.1 System improvements

The results from NEEM test ice measurements were significantly more variable than dry standard in rods test. The main difference between NEEM test ice extraction and dry standard in rod test is the presence of water vapor. This result suggests that the presence of water vapor exacerbate alteration of sample gas in the rods and the sample line do not adequately trap H₂O. As such, enlarging the H₂O trap capacity or installing a second H₂O trap is necessary.

The dry standard in rod test shows rather significant variability, which suggests that the sample gas is altered in the rods. Following recommendation from colleagues at Scripps Institute of Oceanography (J. Severinghaus, R. Beaudette, personal communication) it might be necessary to “bake” the stainless steel rods. This procedure involves taking the rods out of the cryocooler, filling the rods with pure O₂, and increasing the temperature of the rods to 300°C. The purpose of this procedure is to passivate and oxidize the stainless steel surface. To further passivate the stainless steel surface, one might consider to do chemical treatment (such as electropolishing) on the rods.

Several improvement suggestions mentioned in this thesis (mainly baking the rods and extra H₂O trap) were implemented by Frøystad (2021). As a result, Frøystad (2021) successfully conducted NEEM test ice measurements that produce reasonable results. Furthermore, successful measurement campaign over Eemian RECAP ice was conducted. The final reported precision and error attribution to various steps were also done by Frøystad (2021).

Other technical challenges were overcome in this project. These challenges include the pumps not operating efficiently at the beginning. This was, at times, due to pumps sitting too long without use so keeping up with oil changes and observing that the diaphragms on the turbomolecular pumps are not decaying can help prevent failure of the pumps.

Leak checks within the lines are important to prevent ambient air from entering the sample collection rods. The Swagelok connectors are reliable but due to the (aforementioned) move of the equipment from Rockefeller to Tagensvej, some of the connections had to be broken and reconnected – causing leaks in the sample line.

The extraction flasks are fragile and need to be stored appropriately. Again, the recent move of the equipment also compromised the connection part at the top of the extraction flasks and repairs with a help of glassblower had to be done.

There were also problems with the cryocooler and the He compressor at the new Tagensvej 16 building. The water-cooling system often shut-off, resulting in overheating of the lines to the He compressor and an eventual tripping of the internal switch. These problems could be solved with an improved electrical system and He compressor within the building.

5 CONCLUSION

At the end of my research schedule, we were successfully able to melt ice and extract gases in the extraction system developed by Reutenauer (2016) but it was not without its difficulties. The extraction system was tested and improved throughout the project to ensure components were in optimal working conditions and not influencing results. Repairs and additions were necessary throughout some areas, for example, a CO₂ trap was added between the standard tank and the MS. The MS scripts and settings were adjusted to ensure the MS was providing accurate results. The two days of measuring NEEM test ice provided results that could be analyzed to focus on where further improvements were needed, in particular in the collection unit. Building from work done in this thesis, Frøystad (2021) was able to successfully measure RECAP ice core at acceptable precision (0,03 per mil for $\delta^{18}\text{O}$ and 0,01 per mil for $\delta^{15}\text{N}$) needed to improve the dating of the Eemian section.

Some of the suggestions made at the conclusion of this project were addressed but further consideration for optimizing and improving the O₂ extraction system will enable higher precision for future measurements.

6 REFERENCES

Baggenstos, D., Bauska, T. K., Severinghaus, J. P., Lee, J. E., Schaefer, H., Buizert, C., Brook, E. J., Shackleton, S., and Petrenko, V. V.: Atmospheric gas records from Taylor Glacier, Antarctica, reveal ancient ice with ages spanning the entire last glacial cycle, 13, 943, 2017.

Bauska, T. K., Baggenstos, D., Brook, E. J., Mix, A. C., Marcott, S. A., Petrenko, V. V., Schaefer, H., Severinghaus, J. P., and Lee, J. E.: Carbon isotopes characterize rapid changes in atmospheric carbon dioxide during the last deglaciation, *PNAS*, 113, 3465–3470, <https://doi.org/10.1073/pnas.1513868113>, 2016.

Beck, J., Bock, M., Schmitt, J., Seth, B., Blunier, T., and Fischer, H.: Bipolar carbon and hydrogen isotope constraints on the Holocene methane budget, 15, 7155–7175, <https://doi.org/10.5194/bg-15-7155-2018>, 2018.

Bender, M., Sowers, T., and Lipenkov, V.: On the concentrations of O₂, N₂, and Ar in trapped gases from ice cores, 100, 18651–18660, 1995.

Blunier, T. and Schwander, J.: Gas enclosure in ice: age difference and fractionation, 307–326, 2000.

Buizert, C., Sigl, M., Severi, M., Markle, B. R., Wettstein, J. J., McConnell, J. R., Pedro, J. B., Sodemann, H., Goto-Azuma, K., Kawamura, K., Fujita, S., Motoyama, H., Hirabayashi, M., Uemura, R., Stenni, B., Parrenin, F., He, F., Fudge, T. J., and Steig, E. J.: Abrupt ice-age shifts in southern westerly winds and Antarctic climate forced from the north, 563, 681, <https://doi.org/10.1038/s41586-018-0727-5>, 2018.

Capron, E., Landais, A., Chappellaz, J., Schilt, A., Buiron, D., Dahl-Jensen, D., Johnsen, S. J., Jouzel, J., Lemieux-Dudon, B., Loulergue, L., Leuenberger, M., Masson-Delmotte, V., Meyer, H., Oerter, H., and Stenni, B.: Millennial and sub-millennial scale climatic variations recorded in polar ice cores over the last glacial period, 6, 345–365, <https://doi.org/10.5194/cp-6-345-2010>, 2010.

Cook, E., Portnyagin, M., Ponomareva, V., Bazanova, L., Svensson, A., and Garbe-Schönberg, D.: First identification of cryptotephra from the Kamchatka Peninsula in a Greenland ice core: Implications of a widespread marker deposit that links Greenland to the Pacific northwest, *Quaternary Science Reviews*, 181, 200–206, <https://doi.org/10.1016/j.quascirev.2017.11.036>, 2018.

Craig, H.: Standard for Reporting Concentrations of Deuterium and Oxygen-18 in Natural Waters, 133, 1833–1834, 1961.

Craig, H., Horibe, Y., and Sowers, T.: Gravitational Separation of Gases and Isotopes in Polar Ice Caps, 242, 1675–1678, <https://doi.org/10.1126/science.242.4886.1675>, 1988.

Dansgaard, W., Johnsen, S. J., Møller, J., and Langway, C. C.: One Thousand Centuries of Climatic Record from Camp Century on the Greenland Ice Sheet, *Science*, 166, 377–380, <https://doi.org/10.1126/science.166.3903.377>, 1969.

Dole, M.: THE RELATIVE ATOMIC WEIGHT OF OXYGEN IN WATER AND IN AIR, *J. Am. Chem. Soc.*, 57, 2731–2731, <https://doi.org/10.1021/ja01315a511>, 1935.

Dyonisius, M. N., Petrenko, V. V., Smith, A. M., Hua, Q., Yang, B., Schmitt, J., Beck, J., Seth, B., Bock, M., Hmiel, B., Vimont, I., Menking, J. A., Shackleton, S. A., Baggenstos, D., Bauska, T. K., Rhodes, R. H., Sperlich, P., Beaudette, R., Harth, C., Kalk, M., Brook, E. J., Fischer, H., Severinghaus, J. P., and Weiss, R. F.: Old carbon reservoirs were not important in the deglacial methane budget, 367, 907–910, <https://doi.org/10.1126/science.aax0504>, 2020.

Emsley, J.: *Nature's Building Blocks: An A-Z Guide to the Elements*, OUP Oxford, 709 pp., 2011.

Faïn, X., Rhodes, R. H., Philip, P., Petrenko, V. V., Fourteau, K., Chellman, N., Crosier, E., McConnell, J. R., Brook, E. J., Blunier, T., Legrand, M., and Chappellaz, J.: Northern Hemisphere atmospheric history of carbon monoxide since preindustrial times reconstructed from multiple Greenland ice cores, 1–28, <https://doi.org/10.5194/cp-2021-28>, 2021.

Frøystad, R.: *Measuring d18O of atmospheric oxygen for synchronizing ice core records*, Masters of Science thesis, University of Copenhagen, Copenhagen, Denmark, 68 pp., 2021.

Grachev, A. M.: ICE CORE RECORDS | Thermal Diffusion Paleotemperature Records, in: *Encyclopedia of Quaternary Science (Second Edition)*, edited by: Mock, S. A. E. J., Elsevier, Amsterdam, 431–434, 2013.

Guillevic, M., Bazin, L., Landais, A., Stowasser, C., Masson-Delmotte, V., Blunier, T., Eynaud, F., Falourd, S., Michel, E., Minster, B., Popp, T., Prié, F., and Vinther, B. M.: Heinrich event 4 in Greenland ice core records, 44, 2014.

Headly, M. A.: *Krypton and xenon in air trapped in polar ice cores: paleo-atmospheric measurements for estimating past mean ocean temperature and summer snowmelt frequency*, UC San Diego, 2008.

Herron, M. M. and Langway, C. C.: Firm densification: an empirical model, 25, 373–385, 1980.

Horibe, Y., Shigehara, K., and C Jr, L. C.: Chemical and isotopic composition of air inclusions in a Greenland ice core, 73, 207–210, 1985.

Jenk, T. M., Rubino, M., Etheridge, D., Ciobanu, V. G., and Blunier, T.: A new set-up for simultaneous high-precision measurements of CO₂, δ¹³C-CO₂ and δ¹⁸O-CO₂ on small ice core samples, *Atmos. Meas. Tech.*, 9, 3687–3706, <https://doi.org/10.5194/amt-9-3687-2016>, 2016.

Joergensen, K.: O₂ Extraction System Schematic Drawing, 2021.

Kageyama, M., Braconnot, P., Harrison, S. P., Haywood, A. M., Jungclaus, J. H., Otto-Bliesner, B. L., Peterschmitt, J.-Y., Abe-Ouchi, A., Albani, S., Bartlein, P. J., Brierley, C., Crucifix, M., Dolan, A., Fernandez-Donado, L., Fischer, H., Hopcroft, P. O., Ivanovic, R. F., Lambert, F., Lunt, D. J., Mahowald, N. M., Peltier, W. R., Phipps, S. J., Roche, D. M., Schmidt, G. A., Tarasov, L., Valdes, P. J., Zhang, Q., and Zhou, T.: The PMIP4 contribution to CMIP6 – Part 1: Overview and over-arching analysis plan, 11, 1033–1057, <https://doi.org/10.5194/gmd-11-1033-2018>, 2018.

Kindler, P.: NGRIP isotopic gas measurements from 10 to 38 kyr and a temperature reconstruction for the last glacial, PhD Thesis, University of Bern, Bern, Switzerland, 187 pp., 2013.

Köhler, P., Nehrbass-Ahles, C., Schmitt, J., Stocker, T. F., and Fischer, H.: A 156 kyr smoothed history of the atmospheric greenhouse gases CO₂, CH₄, and N₂O and their radiative forcing, 9, 363–387, <http://dx.doi.org/10.5194/essd-9-363-2017>, 2017.

Landais, A., Barnola, J. M., Masson-Delmotte, V., Jouzel, J., Chappellaz, J., Caillon, N., Huber, C., Leuenberger, M., and Johnsen, S. J.: A continuous record of temperature evolution over a sequence of Dansgaard-Oeschger events during Marine Isotopic Stage 4 (76 to 62 kyr BP), 31, <https://doi.org/10.1029/2004GL021193>, 2004.

Lynch-Stieglitz, J.: The Atlantic Meridional Overturning Circulation and Abrupt Climate Change, 9, 83–104, <https://doi.org/10.1146/annurev-marine-010816-060415>, 2017.

Masson-Delmotte, V., Steen-Larsen, H. C., Ortega, P., Swingedouw, D., Popp, T., Vinther, B. M., Oerter, H., Sveinbjornsdottir, A. E., Gudlaugsdottir, H., Box, J. E., Falourd, S., Fettweis, X., Gallée, H., Garnier, E., Gkinis, V., Jouzel, J., Landais, A., Minster, B., Paradis, N., Orsi, A., Risi, C., Werner, M., and White, J. W. C.: Recent changes in north-west Greenland climate documented by NEEM shallow ice core data and simulations, and implications for past-temperature reconstructions, *The Cryosphere*, 9, 1481–1504, <https://doi.org/10.5194/tc-9-1481-2015>, 2015.

NEEM Community Members: Eemian interglacial reconstructed from a Greenland folded ice core, *Nature*, 493, 489–494, <https://doi.org/10.1038/nature11789>, 2013.

Nehrbass-Ahles, C., Shin, J., Schmitt, J., Bereiter, B., Joos, F., Schilt, A., Schmidely, L., Silva, L., Teste, G., Grilli, R., Chappellaz, J., Hodell, D., Fischer, H., and Stocker, T. F.: Abrupt CO₂ release to the atmosphere under glacial and early interglacial climate conditions, 369, 1000–1005, <https://doi.org/10.1126/science.aay8178>, 2020.

Nicewonger, M. R., Aydin, M., Prather, M. J., and Saltzman, E. S.: Reconstruction of Paleofire Emissions Over the Past Millennium From Measurements of Ice Core Acetylene, 47, e2019GL085101, <https://doi.org/10.1029/2019GL085101>, 2020.

Oyabu, I., Kawamura, K., Kitamura, K., Dallmayr, R., Kitamura, A., Sawada, C., Severinghaus, J. P., Beaudette, R., Orsi, A., Sugawara, S., Ishidoya, S., Dahl-Jensen, D., Goto-Azuma, K., Aoki, S., and Nakazawa, T.: New technique for high-precision, simultaneous measurements of CH₄, N₂O and CO₂ concentrations; isotopic and elemental ratios of N₂, O₂ and Ar; and total air content in ice cores by wet extraction, 13, 6703–6731, <https://doi.org/10.5194/amt-13-6703-2020>, 2020.

Petrenko, V. V., Severinghaus, J. P., Brook, E. J., Reeh, N., and Schaefer, H.: Gas records from the West Greenland ice margin covering the Last Glacial Termination: a horizontal ice core, *Quaternary Science Reviews*, 25, 865–875, <https://doi.org/10.1016/j.quascirev.2005.09.005>, 2006.

Rasmussen, S. O., Abbott, P. M., Blunier, T., Bourne, A. J., Brook, E., Buchardt, S. L., Buizert, C., Chappellaz, J., Clausen, H. B., Cook, E., Dahl-Jensen, D., Davies, S. M., Guillevic, M., Kipfstuhl, S., Laepple, T., Seierstad, I. K., Severinghaus, J. P., Steffensen, J. P., Stowasser, C., Svensson, A., Vallenga, P., Vinther, B. M., Wilhelms, F., and Winstrup, M.: A first chronology for the North Greenland Eemian Ice Drilling (NEEM) ice core, *Clim. Past*, 9, 2713–2730, <https://doi.org/10.5194/cp-9-2713-2013>, 2013.

Reutenauer, C.: Measuring the triple O₂ isotopic composition of air trapped in ice cores and quantifying the causes of $\delta^{18}\text{O}_{\text{atm}}$ millennial scale variations, PhD Thesis, University of Copenhagen, Copenhagen, Denmark, 321 pp., 2016.

Rhodes, R. H., Brook, E. J., Chiang, J. C., Blunier, T., Maselli, O. J., McConnell, J. R., Romanini, D., and Severinghaus, J. P.: Enhanced tropical methane production in response to iceberg discharge in the North Atlantic, 348, 1016–1019, 2015.

Schmitt, J., Schneider, R., and Fischer, H.: A sublimation technique for high-precision measurements of $\delta^{13}\text{C}_{\text{CO}_2}$ and mixing ratios of CO₂ and N₂O from air trapped in ice cores, *Atmos. Meas. Tech.*, 4, 1445–1461, <https://doi.org/10.5194/amt-4-1445-2011>, 2011.

Schwander, J.: The transformation of snow to ice and the occlusion of gases, *The Environmental Record in Glaciers and Ice Sheets*, edited by: Oeschger, H. and Langway, CC, Wiley, New York, 1989.

Seltzer, A. M., Buizert, C., Baggenstos, D., Brook, E. J., Ahn, J., Ji-Woong, Y., and Severinghaus, J. P.: Does $\delta^{18}\text{O}$ of O_2 record meridional shifts in tropical rainfall?, 13, 1323, 2017.

Severinghaus, J. P., Grachev, A., Luz, B., and Caillon, N.: A method for precise measurement of argon $40/36$ and krypton/argon ratios in trapped air in polar ice with applications to past firn thickness and abrupt climate change in Greenland and at Siple Dome, Antarctica, *Geochimica et Cosmochimica Acta*, 67, 325–343, [https://doi.org/10.1016/S0016-7037\(02\)00965-1](https://doi.org/10.1016/S0016-7037(02)00965-1), 2003.

Severinghaus, J. P., Beaudette, R., Headly, M. A., Taylor, K., and Brook, E. J.: Oxygen-18 of O_2 Records the Impact of Abrupt Climate Change on the Terrestrial Biosphere, *Science*, 324, 1431–1434, <https://doi.org/10.1126/science.1169473>, 2009.

Shackleton, S., Baggenstos, D., Menking, J. A., Dyonisius, M. N., Bereiter, B., Bauska, T. K., Rhodes, R. H., Brook, E. J., Petrenko, V. V., McConnell, J. R., Kellerhals, T., Häberli, M., Schmitt, J., Fischer, H., and Severinghaus, J. P.: Global ocean heat content in the Last Interglacial, 13, 77–81, <https://doi.org/10.1038/s41561-019-0498-0>, 2020.

Simonsen, M. F., Baccolo, G., Blunier, T., Borunda, A., Delmonte, B., Frei, R., Goldstein, S., Grinsted, A., Kjær, H. A., and Sowers, T.: East Greenland ice core dust record reveals timing of Greenland ice sheet advance and retreat, 10, 1–8, 2019.

Slater, C., Preston, T., and Weaver, L. T.: Stable isotopes and the international system of units, 15, 1270–1273, <https://doi.org/10.1002/rcm.328>, 2001.

Sowers, T., Bender, M., and Raynaud, D.: Elemental and isotopic composition of occluded O_2 and N_2 in polar ice, 94, 5137–5150, 1989.

Sowers, T., Brook, E., Etheridge, D., Blunier, T., Fuchs, A., Leuenberger, M., Chappellaz, J., Barnola, J. M., Wahlen, M., Deck, B., and Weyhenmeyer, C.: An interlaboratory comparison of techniques for extracting and analyzing trapped gases in ice cores, 102, 26527–26538, <https://doi.org/10.1029/97JC00633>, 1997.

Stocker, T. F. and Johnsen, S. J.: A minimum thermodynamic model for the bipolar seesaw, *Paleoceanography*, 18, 1087, <https://doi.org/10.1029/2003PA000920>, 2003.

WAIS Divide Project Members: Precise inter-polar phasing of abrupt climate change during the last ice age, *Nature*, 520, 661–665, <https://doi.org/10.1038/nature14401>, 2015.

Wang, Y. J., Cheng, H., Edwards, R. L., An, Z. S., Wu, J. Y., Shen, C.-C., and Dorale, J. A.: A High-Resolution Absolute-Dated Late Pleistocene Monsoon Record from Hulu Cave, China, 294, 2345–2348, <https://doi.org/10.1126/science.1064618>, 2001.